Cement and Concrete Research 142 (2021) 106351

Contents lists available at ScienceDirect

Cement and Concrete Research

journal homepage: www.elsevier.com/locate/cemconres

Chemistry of the interaction between an alkoxysilane-based impregnation treatment and cementitious phases

I. Garcia-Lodeiro [a,*], P.M. Carmona-Quiroga [a], Rafael Zarzuela [b], Maria J. Mosquera [b], M. T. Blanco-Varela [a]

[a] Eduardo Torroja Institute (CSIC), 28033 Madrid, Spain
[b] TEP-243 Nanomaterials Group, Department of Physical-Chemistry, Faculty of Science, University of Cadiz, 11510 Puerto Real, Spain

ARTICLE INFO

Keywords:
Impregnation treatment
Consolidation
Alkoxysilane
Cement
C-S-H gel
NMR

ABSTRACT

Chemical compatibility with a wide range of materials is among the features that has driven the use of alkoxysilanes as consolidants in built structures. Such compatibility is particularly important in cementitious materials where the reaction with portlandite may generate C-S-H gel, one of the main hydration phases of OPC. The cementitious matrix is a complex system, however, and the reaction of its many phases with alkoxysilanes, while poorly understood, may determine treatment efficacy. This article describes a detailed study of the individual interactions between an oligomeric alkoxysilane-based impregnation treatment previously shown to interact with the portlandite present in cement paste and the cementitious phases generated in ordinary portland cement hydration.

The findings show that both portlandite and C-S-H gel interact with the silicon oligomers in the hydrolysed impregnation treatment to generate a C-S-H gel (in the case of portlandite) and a rise in C-S-H gel mean chain length (MCL). Ettringite is also altered in the presence of alkoxysilanes, transforming to gypsum and AH_3. Its transformation generates a tetrahedral aluminium that is taken up into a high silicon gel sourced from the treatment to form an amorphous aluminosilicate gel. Monocarboaluminate and katoite also partially decompose in the interaction with the product, whereas gibbsite remains unaffected.

1. Introduction

Surface consolidation, one of the stages in restoring porous construction materials such as stone and concrete [1–3], consists in applying a product to recover the properties of degraded materials or heighten the resistance of their surfaces after cleaning. Consolidants penetrate deeply into the construction material through its pore structure, improving internal cohesion and rendering the deteriorated surface layer more robust and adherent.

European standard EN-1504-2 describes three groups of surface protection treatments. (1) Coatings (resins, cementitious veneering…) form a surface layer on the material to protect it from the ingress of aggressive species or enhance its mechanical strength. (2) Hydrophobic impregnations (siloxanes, synthetic wax…) penetrate the pore structure, preventing water and hydro-soluble substances from entering the material. (3) Impregnations (alkoxysilanes, inorganic nanoparticles, alkaline silicates…) penetrate the material and react in its interior to form a more compact and stronger structure. Oligomeric or monomeric colloidal silica-based compounds (hereafter oligo/monomeric silica sols) such as tetraethoxysilanes (also known as tetraethyl orthosilicates or TEOS) are the consolidants most widely used to protect building façades.

Thanks to their scant viscosity, oligo/monomeric silica sols are able to penetrate the pore structure of construction materials. After hydrolysis they condense to form an amorphous silica [4–6]. Hydrolysis begins inside the pores where the sol reacts with water vapour or the water adsorbed onto the pore walls to form silicic acid containing highly reactive silanol groups and ethanol (Eq. (1), TEOS hydrolysis). After hydrolysis the ethanol evaporates and the Si-OH groups react and condense, giving rise to siloxane (Si-O-Si) bonds and ultimately to a three-dimensional silica gel (Eq. (2)).

$$Si(OC_2H_5) + 4\,H_2O \rightarrow Si(OH)_4 + CH_3 - CH_2OH \quad (1)$$

$$Si(OH)_4 \rightarrow SiO_2 + 2H_2O \quad (2)$$

* Corresponding author.
E-mail address: iglodeiro@ietcc.csic.es (I. Garcia-Lodeiro).

https://doi.org/10.1016/j.cemconres.2020.106351
Received 24 July 2020; Received in revised form 15 December 2020; Accepted 19 December 2020
Available online 16 January 2021

That reactivity makes alkoxysilanes particularly apt for use in construction materials containing siliceous components, for the silanol groups present in the walls of the substrate's pore structure react with the products of TEOS hydrolysis, generating very strong siloxane bonds and raising internal cohesion in the former [7–9].

Despite the advantages featured by these products, namely suitable viscosity, surface tension, density and gelling time and their compatibility with many construction materials, they are also characterised by a series of drawbacks. These include differences between the thermal expansion coefficient of silica xerogel and other materials, the former's scant reactivity with carbonate-based materials and primarily their small pore size (micropores). That pore structure exposes the xerogel to high capillary pressure (ΔP is inversely proportional to pore radius) during drying, inducing shrinkage and cracking and hindering mechanical strength development. Researchers have adopted a number of approaches to improve gel properties, some based on including inorganic oxide nanoparticles [10,11] and others on the use of surfactants [12,13]. Adding particles, although effective, is less versatile because the additives may alter the colour of the materials treated. In an earlier study, the authors developed an impregnation product [14] by combining a sol-gel procedure with ultrasonic stirring in which an oligomeric silica precursor was micro-emulsified in n-octylamine surfactant-stabilised water. That product gels in keeping with a reverse micelles-mediated mechanism, forming a fissure-free, monolithic nanostructured gel with mesopores of a uniform size. Such synthetic products have been proven to interact effectively with and bond tightly to carbonatic substrates [15].

Although the mechanisms governing alkoxysilane interaction with a number of types of natural stone have been widely studied and are generally understood, those processes may differ significantly in cementitious materials due to the chemical conditions prevailing. In the medium basicity of portland cement concretes or mortars, the presence of hydroxyls groups condition the hydrolysis and condensation stages of the sol-gel reaction [5,6]. At the same time, the presence of calcium ions in the pore solution in such material favours precipitation of the primary component portland cement-based products, C-S-H gel (Eq. (3)), which may enhance the chemical compatibility between the reaction products and the substrate. According to Barberena-Fernández et al. [16], TEOS effectively consolidate portland cement mortars because they raise their mechanical strength and reduce their porosity and permeability without significantly altering colour. Pigino et al. [17], in turn, observed lower capillary absorption and lower chloride migration and surface carbonation rates in concretes treated with a TEOS-based sol.

$$Ca(OH)_2 \text{ (from OPC hydration)} + Si(OH)_4 \text{ (from TEOS)} \rightarrow C-S-H \text{ gel} \quad (3)$$

In addition to a basic pH and the presence of portlandite, hydrated cement paste is characterised by different phases with hydroxyl groups in their structure, including hydrated calcium sulfoaluminates such as ettringite and AFm phases, calcium silicate hydrate (C-S-H) and aluminates, ferrites and calcium silicates comprising the anhydrous phase of cement. Therefore, alkoxysilane consolidation may proceed not only as in Eqs. (1) and (2), but by reacting with the cement paste phases themselves. In light of the complexity of cementitious materials, an understanding is needed of all such potential chemical interactions and reactions, for impregnation product compatibility and efficacy ultimately depend on the reaction products forming.

A number of studies have shown that TEOS and their derivatives react with portlandite to produce C-S-H gel [16,18–22]. The oligomeric alkoxysilane-based product developed by the authors exhibited similar reactivity with portlandite and hydrated cement paste, together not only with portlandite consumption but with a lengthening of the Si—O chains in the C-S-H gel [20]. Nonetheless, nothing is known about the interaction between alkoxysilanes and the other phases comprising hydrated cement paste, for given the complexity of the cement system, the effects overlap. This study consists in a detailed exploration of the interaction between an oligomeric alkoxysilane-based TEOS derivative (hereafter UCA-T) and the phases present in portland cement hydration. The interactions were differentiated by separately analysing the chemical reaction between the product and a number of synthetic phases, including portlandite, a synthetic C-S-H gel, a synthetic paste generated by hydrating synthetic C_3S (comprising C-S-H + $Ca(OH)_2$), ettringite, monocarboaluminate, katoite and gibbsite. However, we have to take into account that some cement hydrated phases are very flexible in stoichiometry under practical conditions, a fact that also has influence on their stability and therefore deviations could arise depending on the different cement types.

2. Experimental

2.1. Substrate preparation

The synthetic phases (substrates) studied are listed in Table 1.

Tricalcium silicate (C_3S) was synthesised from a mix of calcium carbonate and silica gel at a CaO/SiO_2 molar ratio of 3. The paste was mixed in a shaker-mixer for 2 h, compressed into wafers, gradually ramped from ambient temperature to 1450 °C, heated at the latter temperature for 5 h and subsequently quenched. That process was repeated until the free lime content declined to under 1%. The material was then ground and sieved to <45 μm. XRD-Rietveld analysis only shows the presence of triclinic polymorph C_3S T1 (pureness >99%), with a high correlation between the observed and calculated patterns (Rwp = 0.13%) [21]. Tricalcium aluminate (C_3A) was synthesised from a mix of calcium carbonate and alumina at a CaO/Al_2O_3 molar ratio of 3 and calcined as C_3S in [21]. Its XRD-Rietveld analysis showed only the cubic polymorph (pureness >99%) and no other calcium aluminates, with lower Ca/Al ratio (such as $C_{12}A_7$ or CA), were identified [23].

Synthetic paste (SP) was prepared by hydrating synthetic C_3S with deionised water (w/c ratio = 0.425). The pastes were mixed manually for 3 min and subsequently cured at 100% RH and a T of 40 °C for 1 year in a controlled N_2 atmosphere [24].

C-S-H gel was synthesised with 2 g of amorphous silica and 250 ml and l of saturated portlandite solution ([CaO] = 17.68 mmol/l; [OH] = 35.36 mmol/l), and stored in air-tight polypropylene beakers at an oven-controlled 40 °C for 60 d. The solution was stirred continuously, maintaining saturation with 5 g of portlandite in semi-permeable bags placed in the beakers, an arrangement that prevented any direct mixing between portlandite and silica. The oven-treated samples were then filtered, immersed in isopropyl alcohol for 2 min, re-filtered and dried in a desiccator at ambient temperature.

Ettringite ($Ca_6Al_2(SO_4)_3(OH)_{12}\cdot 26H_2O$) was synthesised following one of the methods proposed by Struble [25], consisting in suspending $Al_2(SO_4)_3\cdot 18H_2O$ (Panreac) and CaO (via $CaCO_3$ decarbonation instead of the $Ca(OH)_2$ cited in the original procedure) at a molar ratio of 1:6 in 1 l of water. The suspension was stirred for 48 h at ambient temperature in an N_2 atmosphere, after which the ettringite was filtered, rinsed in isopropanol and dried in a desiccator at ambient temperature. According to Rietveld refinement phase quantification, the synthetic ettringite was 98.66% pure, with the remaining 1.34% consisting of mixture of gypsum

Table 1
Wafers prepared with the synthetic phases, substrate weight and amount of impregnation treatment applied.

Substrate	Name	Substrate (g)	UCA-T (g)
Portlandite	$Ca(OH)_2$	0.1572	0.0360
C-S-H gel	CSH	0.1052	0.0422
Synthetic paste	SP	0.1536	0.0370
Ettringite	E	0.1050	0.0413
Monocarboaluminate	MC	0.1210	0.0374
Katoite	K	0.1781	0.0373
Gibbsite	AH_3	0.2627	0.0442

and gibbsite (Rwp = 8.60%) [26].

Katoite, $Ca_3Al_2(OH)_{12}$, (C_3AH_6) was prepared by hydrating synthetic C_3A for 9 d at 25 °C. A post-hydration Rietveld analysis revealed that 79% of the product was katoite and the remaining phase was anhydrous C_3A.

Monocarboaluminate, $Ca_4Al_2(CO_3)(OH)_{12}{\cdot}5H_2O$ ($C_4Ac{\cdot}11H_2O$) was prepared by mixing C_3A and $CaCO_3$ in stoichiometric proportions with distilled water at a liquid/solid ratio of 20/1 by weight. The mix was stirred magnetically and constantly at 25C for 7 d in a sealed beaker, subsequently filtered, rinsed with isopropyl alcohol and dried in a desiccator for 10 d. A TG/DTG analysis revealed that around 77% of the sample was monocarboaluminate, the remaining 23% a mixture of calcite, C_3A, gibbsite and katoite.

The portlandite, $Ca(OH)_2$, (CH) and gibbsite ($Al(OH)_3$), (AH_3) used were >99.5% pure laboratory reagents supplied by MERCK.

2.2. Synthesis of the impregnation product

The impregnation product was synthesised further to an ultrasonication-mediated pathway described in earlier papers [14,20]. It involved mixing 500 ml of an oligomeric silica precursor (TES40, supplied by Wacker, Germany) with 2.5 ml of deionised water and 0.8 ml of n-octylamine (99%, supplied by Sigma-Aldrich) as a surfactant and catalyst. According to manufacturer specifications, TES40 contains a mix of TEOS oligomers with a mean chain length of five Si—O units. The mix was immediately stirred for 10 min in a Bandelin HD3200 ultrasonic probe operating at 74% amplitude.

2.3. Procedure and analysis

The phases described were pressed into 10 mm diameter wafers approximately 1 mm thick. The amounts of UCA-T required to reach saturation (Table 1) were applied drop-by-drop, covering the entire upper surface of each wafer. The samples were then set in a reactor vessel (23 °C, >90% RH) with a layer of deionised water at the bottom and purged with N_2 to establish a controlled, CO_2-free atmosphere. After 21 d, the time recommended for the UCA-T sol-gel reaction [20], the wafers were ground and the interaction of each phase with the consolidant was analysed with XRD, FTIR, TG/DTG and ^{29}Si and ^{27}Al MAS NMR.

UCA-T (sol) was stored under the same experimental conditions and after 21 d the polymerised xerogel was likewise analysed with XRD, FTIR, TG/DTG and ^{29}Si MAS NMR.

XRD analyses were performed on a Bruker D8 Advance diffractometer consisting in a 2.2 kW generator, a copper anode X-ray tube (CuKα1 radiation: 1.5406 Å and CuKα2: 1.5444 Å) operating at 40 kV and 30 mA and fitted with a 0.5° fixed divergence slit and a non-monochromatic Lynxeye superspeed detector bearing a 3 mm anti-scatter slit, a 2.5° Soller slit and a 0.5% Ni K-beta filter. Readings were taken for approximately 1 h per diffractogram over an angular range of 5° to 60° with a 0.02° step size. Infrared spectra were recorded (10 scans) for KBr pellets on a Nicolet 6700 spectrometer in the 4000 cm^{-1} to 400 cm^{-1} range at a spectral resolution of 4 cm^{-1}.

Thermogravimetric heat flow was determined on a TA SDT Q600 analyser with platinum crucibles (empties were used as a reference). The samples were ramped at 4 °C/min to 1000 °C (1050 °C in ettringite) in a nitrogen atmosphere.

NMR analysis was performed on a Bruker Avance III 400 MHz nuclear magnetic resonance (NMR) mass spectrometer under the following conditions: ^{29}Si resonance frequency, 79.5 MHz; spinning rate, 10 kHz; pulse sequence, single 5 μs pulse and 10 s recycle delay; number of transients, 4912; and external standard, tetramethylsilane (TMS); ^{27}Al resonance frequency, 104.3 MHz; spinning rate, 10 kHz; pulse sequence, 2 μs single pulse and 5 s recycle delay; number of transients, 400; and external standard $Al(H_2O)_6^{3+}$.

3. Results and discussion

3.1. Sol-gel product characterisation

As the gelled and cured UCA-T composition and structure were described in an earlier article [20], this section contains only a brief discussion of its characterisation after curing under the same conditions as the synthetic samples (T = 25 °C; RH > 95%; t = 21 d). The findings are intended to serve as a reference for determining both how the substrate modifies silica precursor hydrolysis and condensation and the possible interaction between substrate and UCA-T. Fuller information is available in the Supplementary material (hereafter SM).

The two humps observed on the diffractogram for the polymerised (21 d) UCA-T gel, ranging from 2θ 5° to 15° and 2θ 15° to 35°, were indicative of the formation of an amorphous silica (SM, Fig. SM1).

The FTIR spectra for both the sol and the 21 d gel obtained under the curing conditions described (band assignments in SM, Table SM1) are reproduced in Fig. 1.

The transparent, colourless monolith formed was not fully polymerised after 21 d, as attested to by the presence of bands attributable to ethoxy and silanol group vibrations. Ethanol evaporated during hydrolysis, lowering the intensity of the C—H stretching bands (2880 cm^{-1} to 3000 cm^{-1}) and the bending bands (1300 cm^{-1} to 1400 cm^{-1}) generated by the CH_3 and CH_2 present in the ethoxy groups in ethyl silicate [4,20,22]. The silanol group Si—O band (970 cm^{-1}) was much less intense in the gel than in the sol sample, denoting condensation. No significant differences were observed in the other bands, with the exception of a slight shift and widening in the band at 1077 cm^{-1} in the sol to 1080 cm^{-1}.

Fig. 2 reproduces the deconvoluted ^{29}Si MAS NMR spectra for both sol (initial) and gel (21 d) stage UCA-T (assignment of the deconvoluted components [27–30] and the respective percentage areas in SM, Table SM2).

Certain differences were observed between the 21 d and initial samples. The signal at −82.43 ppm attributed to Q^0 units disappeared and the area of the signals at −96.67 ppm (Q^2) and −103.52 ppm (Q^3) was smaller than in the non-polymerised UCA-T (SM, Table SM2). In addition, two new, very wide signals appeared at −101 ppm (7.51% of the total area) and −111 ppm (29.34%), respectively assigned to Q^3 units with silanol groups (Si-OH) and Q^4 units (SiO_4) (SM, Table SM2). Curing temperature, relative humidity and time significantly conditioned oligomer hydrolysis and condensation: after 3 weeks only around 38% of the silicon had condensed to form a silica gel with a Q^4 or Q^3 structures. In earlier studies the authors observed the oligomer cured at 20 °C and 40% RH for 60 d [20] to generate bands in the same position

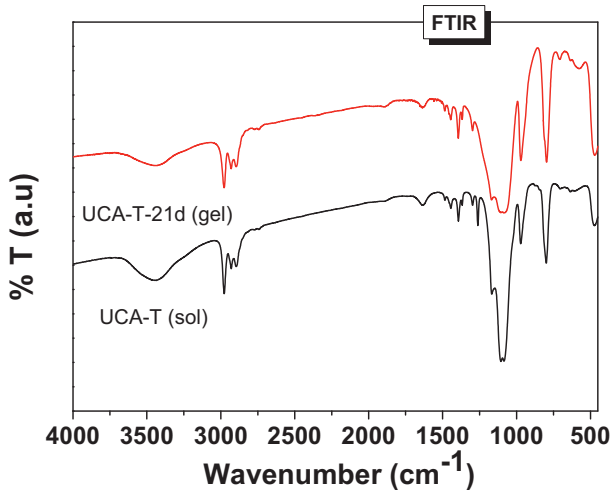

Fig. 1. FTIR spectra for UCA-T (sol) and UCA-T-21 d gel.

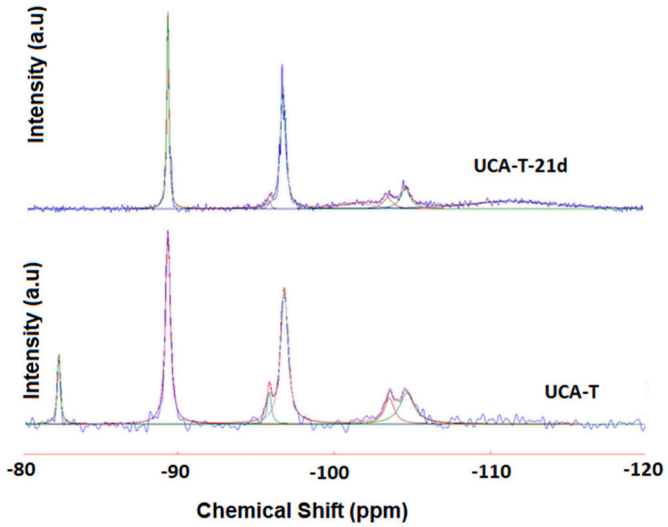

Fig. 2. Deconvoluted ^{29}Si MAS NMR spectra for: below, UCA-T (sol); and above, 21 d (gel) (UCA-T-21d) (legend: blue line represents the original NMR spectrum; red line represents the adjustment after the deconvolution process). (For interpretation of the references to colour in this figure legend, the reader is referred to the web version of this article.)

but with hydrolysis and condensation in a much more advanced stage, with 54% of the Si forming the three-dimensional structure characteristic of xerogels. Alkoxysilane hydrolysis and condensation is a very well understood process whose rate of reaction depends on ambient temperature and relative humidity as well as on the substrate to which the product is applied [4,27,28]. Although a priori, higher ambient relative humidity such as used here may accelerate hydrolysis, a saturated system in a closed environment may deter evaporation of the water generated in the sol-gel reaction, shifting equilibrium away from the condensation stage.

TG (Fig. 3) showed 65.80% total mass loss, with SiO_2 accounting for 34.2% of the mass of the xerogel analysed. That lower percentage than the nominal 40% of SiO_2 present in UCA-T may be due to two factors; i) UCA-T gel has a substantial amount of adsorbed water due to its large specific surface and ii) it contained large amounts of entrained water (sol-gel reaction by-product) in its pores. The DTG curve, in turn, had peaks at 227 °C, 299 °C and 544 °C. The first, accounting for the greatest mass loss and overlapping with the second, was attributed to the loss of water and ethanol [20], whereas the other two less intense peaks might denote pyrolysis of the organic matter (Et groups) in the sample. In light of the distribution of the ethoxy groups bound to the Si as inferred by the

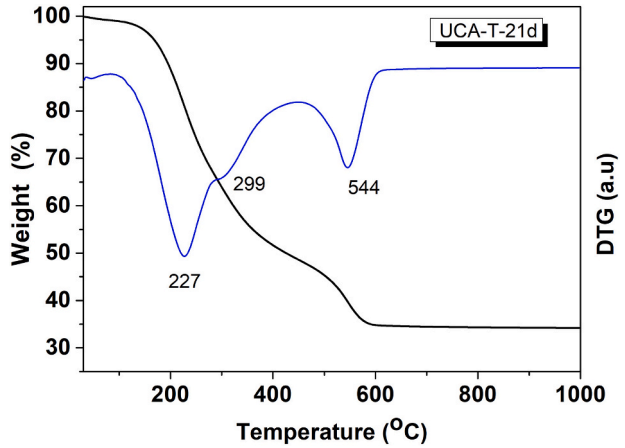

Fig. 3. TG and DTG curves for polymerised UCA-T-21d.

^{29}Si MAS NMR findings and the amount of SiO_2 in the xerogel, the ethoxy group loss during thermal treatment would come to 26% (SM, Table SM17). That is consistent with the mass loss at over 320 °C observed in TG and confirms that not only water and ethanol groups but Si-bound ethoxy groups were released at 299 °C.

3.2. Synthetic phase - UCA-T interaction

3.2.1. Interaction between portlandite and UCA-T

Portlandite crystallises in the trigonal system in the form of hexagonal plates. It is characterised by a layered structure comprising distorted edge-sharing CaO_6 octahedra. Each hydroxyl group bonds to three Ca atoms in its layer and is surrounded by a further three in the adjacent layer [31]. Equilibrium pH is 12.472, solubility product ($\log_{10}K_{sp}$), 22.82 ($Ca(OH)_2 + 2H^+ = Ca^{2+} + 2H_2O$), and calcium concentration under those conditions, 20.36 mmol/l [32].

The diffractograms for the original and UCA-T-treated portlandite wafers (after 21 d in the desiccator at 25 °C and >99% RH) are reproduced in Fig. 4(a). The intensity of the portlandite lines was observed to decline and the intensity of the calcite reflections to rise in the latter, denoting slight carbonation in at least part of the portlandite, despite the N_2 atmosphere prevailing in the desiccator.

The near imperceptibility of the UCA-T bands on the FTIR spectra (Fig. 4(b)) for the $Ca(OH)_2$-UCA-T-21d sample was an indication that portlandite stimulated oligomer hydrolysis significantly and favoured its polymerisation via a different pathway to oligomer self-condensation. The band at 3640 cm^{-1} in the 4000 cm^{-1} to 2000 cm^{-1} zone, attributable to portlandite OH vibrations [33,34], along with a group of very low intensity bands in the 3000 cm^{-1} to 2700 cm^{-1} region reflecting the vibrations generated by the C—H in the original product [20] and/or residual ethanol (from hydrolysis) trapped in the pores, confirmed that hydrolysis had practically finalised after 21 d. In the 2000 cm^{-1} to 400 cm^{-1} region on the spectrum for the $Ca(OH)_2$-UCA-T-21d sample, the primary band at 1420 cm^{-1} was assigned to carbonate asymmetric stretching vibrations [33] (the result of handling-related weathering). A second band in the region, at 966 cm^{-1}, was identified as characteristic of the asymmetric stretching vibrations generated by the Si—O in C-S-H gel [34], while a third at 810 cm^{-1} was attributed to the gel's symmetric stretching vibrations [34]. The second band bore shoulders at 1004 cm^{-1} and 1042 cm^{-1} [34,35], frequencies characteristic of high silicon gels that could not be associated with unreacted xerogel present in the original product in light of the substantial shift in the main band for that compound from 1080 cm^{-1} [20] to lower frequencies (SM, Table SM3).

The TG/DTG curves for the original portlandite and the $Ca(OH)_2$-UCA-T-21d sample are reproduced in Fig. 5. The mass loss in the 400 °C to 550 °C range on the TG/DTG curves for the untreated portlandite exhibited denoted portlandite dehydroxylation, and the loss at 550 °C to 800 °C, $CaCO_3$ decarboxylation [36,37]. The inference of the latter finding was that the original reagent was slightly carbonated, by an estimated ~8% (SM, Table SM4).

The TG curve for sample $Ca(OH)_2$-UCA-T-21d showed continuous mass loss (20.15% up to 200 °C) between 25 °C and 1000 °C, although the rate of loss varied with temperature. The DTG curve exhibited intense mass loss at around 83 °C (steep endothermal peak), attributable either to the loss of absorbed water or dehydration of the C-S-H gel [36,37] resulting from the portlandite - UCA-T reaction (SM, Table SM4). A 2.13% mass loss was recorded between 250 °C and 395 °C (probably water from C-S-H gel). Two other prominent signals were present: between 305 °C and 550 °C, with a 10.90% loss attributed to portlandite dehydroxylation and a second at 550 °C to 750 °C, accounting for 3.8% mass loss associated with carbonate decarbonation (SM, Table SM4). The shift to higher temperatures and the asymmetry of the exothermal peak assigned to portlandite dehydroxylation may be an indication of UCA-T-induced structural change in that phase. None of the endothermal / mass loss signals from 225 °C to 546 °C on the 21 d polymerised UCA-T curves (Fig. 3) were observed, inferring that

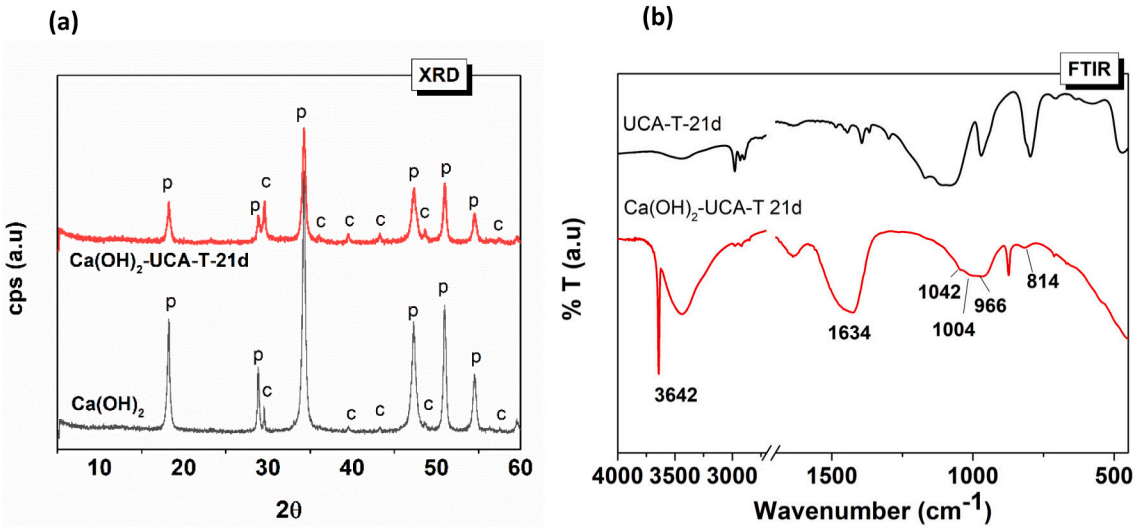

Fig. 4. (a) XRD patterns for $Ca(OH)_2$ and $Ca(OH)_2$-UCA-T-21d (legend: p, portlandite [$Ca(OH)_2$ (COD 2101033)]; c, calcite [$CaCO_3$ (COD 9000095)]); and (b) FTIR spectra for UCA-T-21d and $Ca(OH)_2$-UCA-T-21d.

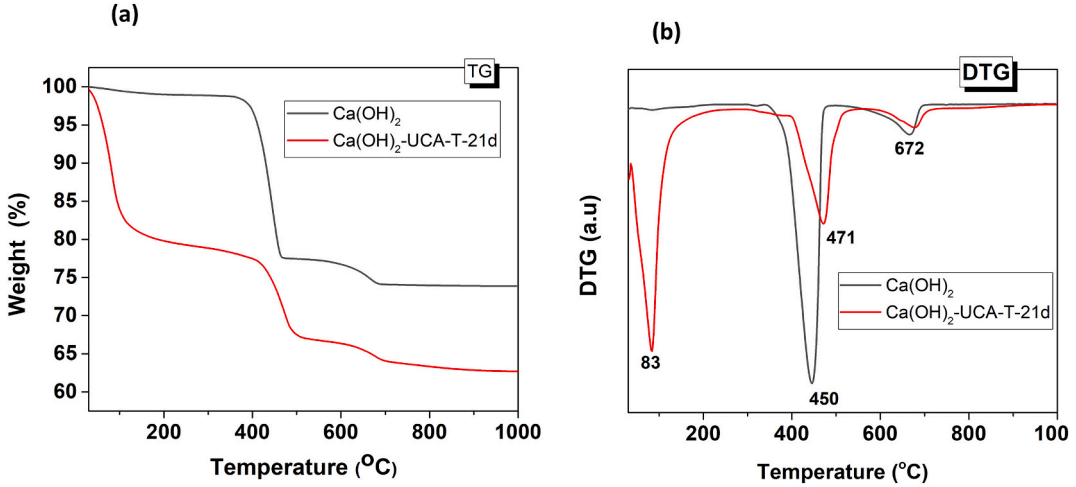

Fig. 5. (a) TG and (b) DTG curves for $Ca(OH)_2$ and $Ca(OH)_2$-UCA-T-21d.

ethoxy group presence in the sample must have been very minor. That observation was consistent with the low intensity of the C—H bands on the FTIR spectra.

The spectrum for sample $Ca(OH)_2$-UCA-T-21d showed slightly higher carbonate content than the original sample (8.04% to 9.21%), indicating less intense UCA-T carbonation might be deduced from the FTIR findings. The steep decline in portlandite content therefore constituted clear proof of its reaction with the impregnation product, forming C-S-H gel as attested to by the FTIR (Fig. 4(b)) and ^{29}Si MAS NMR (SM, Fig. SM2) findings. The ^{29}Si MAS NMR spectrum contained the standard C-S-H units at −79 ppm and −85 ppm, with a prevalence of Q^1 units (associated with end-of-chain silica dimers or tetrahedra) for a mean chain length of 2.7. None of the signals generated after product polymerisation (Fig. 2) was identified separately, confirming that the pH sufficed to break the alkoxysilane oligomers down into their constituent monomers, which would then effectively react with portlandite to produce dimer-heavy C-S-H-like structures.

Overall, $Ca(OH)_2$-UCA-T-21-d characterisation was consistent with the authors' earlier reports [20] confirming the formation of a similar reaction product consisting in a C-S-H gel with an mean chain length (MCL) of 2.5 Si—O units (further to ^{29}Si MAS NMR measurements) and a characteristic 'foil-like' morphology (further to TEM analysis).

3.2.2. *Interaction between synthetic C-S-H gel and UCA-T*

C-S-H gel is a quasi-amorphous, short-range order calcium silicate hydrate. It consists in dreierketten silicate chains bound to a layer of calcium oxide or hydroxide, similar to the structures of tobermorite or jennite [38]. C-S-H gel contains hydroxyl groups in its structure and water in the interlayers. It exhibits variable stoichiometry and a pH that rises with the Ca/Si ratio. At a Ca/Si ratio of 0.6 and a T of 22 °C, its equilibrium pH is around 10, its solubility product ($\log_{10}K_{sp}$) around 9 ($Ca_{0.69}SiO_{2.415}(OH)_{0.55}.0.68H_2O + 0.355H_2O + 1.38H^+ = 0.69Ca^{++} + H_4SiO_4$ dissolution) and calcium concentration 1.2 mmol/l [39]. At a Ca/Si ratio of 0.8 its pH is 10.88 and Ca concentration is 1.23 mmol/l and at a Ca/Si ratio of 1.6 pH is approximately 12.5, the solubility product ($\log_{10}K_{sp}$) 24 and Ca concentration 20.6 mmol/L ($Ca_{1.41}SiO_{2.96}(OH)_{0.90}$:$1.12H_2O + 2.82H^+ = 1.41Ca^{++} + 0.98H_2O + H_4SiO_4$) [40].

The diffractogram for the pre-treatment C-S-H gel (See Fig. 6) exhibited a series of reflections associated with highly amorphous tobermorite [41], at 2θ values of 29.26°, 31.82°, 49.7° and 55.15°. After treatment with UCA-T, the XRD pattern contained a series of additional signals associated with calcite formation.

The FTIR spectrum for untreated C-S-H (Fig. 7(a)) had a band characteristic of O—H stretching at 3442 cm^{-1} and another of the

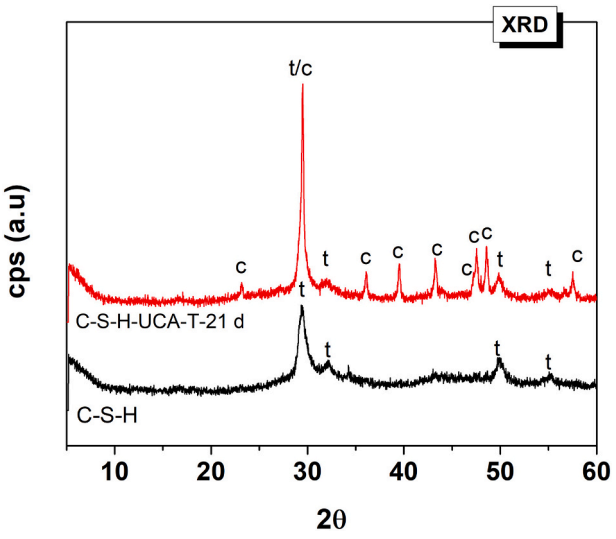

Fig. 6. XRD pattern for C-S-H and C-S-H-UCA-T-21d (legend: C, calcite (COD 9000095); t, tobermorite (COD 9002245)).

bending vibrations associated with water in the gel at 1641 cm^{-1} [33] (SM, Table SM5). A small shoulder was observed at around 3642 cm^{-1}, perhaps associated with the O—H stretching vibrations in amorphous portlandite [33,34]. The Si—O asymmetric stretching band associated with C-S-H gel located at 966 cm^{-1} [34] was highly asymmetric and overlapped with signals at 1040 cm^{-1} and 1200 cm^{-1}, associated with Si—O vibrations in more polymerised structures [35]; the O-Si-O bending band, also wide and asymmetric, was positioned at 452 cm^{-1}. C—O asymmetric stretching vibrations generated a very wide band between 1400 cm^{-1} and 1500 cm^{-1}, which would be attributable not only to calcite (1427 cm^{-1}) but also to more amorphous calcium carbonates whose C—O asymmetric stretching bands were located at 875 cm^{-1}, overlapping with another at 860 cm^{-1}. The original C-S-H was therefore slightly carbonated.

The FTIR spectrum for sample C-S-H-UCA-T-21d had no -CH_3- or -CH_2-related C—H stretching bands (Fig. 7(a)), an indication of UCA-T hydrolysis. The ν_{as} band at 969 cm^{-1} and the δ O-Si-O band at 454 cm^{-1} were unaltered, while an intense band was observed at 1054 cm^{-1}, overlapping with the gel's primary band, which was not the same as the 21 d gelled UCA-T band (Fig. 7(b)). After spectrum subtraction, however (Fig. 7(c)), the new band at 1054 cm^{-1} shifted to 1069 cm^{-1} and the band at 452 cm^{-1} to 464 cm^{-1}, values much closer to those observed for UCA-T after 21 d gelling, and the Si—O symmetric stretching band at 781 cm^{-1} was much more pronounced. The carbonate bands narrowed and the C—O ν_3 band shifted to lower wavenumbers on the C-S-H-UCA-T-21d spectrum, denoting further carbonation during interaction with the impregnation treatment.

The TG/DTG curves for the original C-S-H gel (Fig. 8) exhibited steep mass loss at around 130 °C (13.78% up to 250 °C) (Fig. 8(b)), mirrored on the DTG curve as an intense endothermal signal attributed to C-S-H gel dehydration [36]. A further 2.1% loss (probably of water present in the gel) was recorded on the DTG curve from 250 °C to 350 °C. That was followed by a very wide endothermal signal with several nadirs, the most intense at 423 °C, signifying mass losses at different rates and interpreted as loss of the water in the gel and dehydroxylation of traces of a possible amorphous portlandite [37], also detected with FTIR. A 7.6% loss was recorded between 350 °C and 600 °C (Fig. 8(a); SM, Table SM6), primarily due to water loss from the gel, for if portlandite were deemed to be the source, the percentage would have been 31% and intense peaks would have appeared on the respective diffractograms and FTIR spectra, which were not in fact observed. A comparison of the enthalpy of this endothermal signal to portlandite enthalpy showed that just 2% at most of the total loss would be attributable to that phase. The endothermal signals recorded through the end of the test may have been associated with mass loss from different carbonates and gel water (3.9%); the exothermal signals at T of >800 °C were not associated with water loss but with the solid state formation of calcium silicates [36]. Total loss amounted to 27.51%.

The total mass loss in sample C-S-H-UCA-T-21d, while somewhat greater than twice the loss observed in the original C-S-H gel (SM, Table SM6), was not due to the decomposition of residual ethoxy groups present in the impregnation product, for the losses did not occur at the same temperature (Fig. 3). The most significant drop (47.58%) took place in the first 250 °C (over three-fold the loss in the original C-S-H gel in the same range: Fig. 8(a); SM, Table SM6) and the highest dehydration rate was recorded at 86 °C, substantially lower than the peak rate at 126 °C found for the original sample. Consequently, sample C-S-H-UCA-T-21d may have absorbed environmental water and/or some water from alkoxysilane hydrolysis and condensation that may have remained in the sample, which consequently had a high free or scantly bound water content. The high specific surface of the possible reaction products, C-S-H and nano-structured silica xerogel, would favour water absorption, particularly under high humidity conditions.

A comparison of the two DTG curves from 200 °C through the end of the test (Fig. 8(b)) revealed the absence of some signals (423 °C) and the appearance of others (a small hump at 600 °C and a tiny peak at 712 °C) on the treated sample, apparently indicating a reaction between UCA-T and an amorphous portlandite possibly present in the original sample (detected with FTIR) and a modification of the carbonates in the sample. Scant mass loss was observed in the 250 °C to 500 °C range, while the loss at 550 °C to 750 °C, associated with carbonate decarbonation, denoted minor sample carbonation.

The deconvoluted ^{29}Si MAS NMR spectra for both the original and the treated (C-S-H-UCA-T-21d) C-S-H gel are reproduced in Fig. 9. The components of the two spectra differed visibly: the C-S-H gel had three, at −79.62 ppm associated with Q^1 units, −83.10 ppm with Q^2(L) units and −85.61 ppm with Q^2 units [42–44] (SM, Table SM7). The signal at −79 ppm practically disappeared on the spectrum for C-S-H-UCA-T-21d, which exhibited a series of bands in the −90 ppm to −103 ppm range associated with Q^3 and Q^4 units, i.e., more polymerised environments [43]. Richardson [44] proposed the use of information derived from different Q^n units to calculate the mean silicate chain length (MCL) of C–S–H gels from the following expression:

$$MCL = 2^{*}\left(Q^{1} + Q^{2}(L) + Q^{2}\right)/Q^{1} \quad (4)$$

In this case the MCL showed a rise from 14 units in the original to ~44 in the treated gel. That may denote interaction between the C-S-H gel and the silicon groups in the polymerised product, entailing UCA-T oligomer uptake into and modification of the C-S-H structure. The presence of such Q^3 and Q^4 units might be thought to be attributable to residual UCA-T that had not reacted after 21 d of polymerisation, although those signals appeared in clearly different positions on the polymerised UCA-T-21d (−103.52 ppm and −104 ppm) spectrum (Fig. SM2, Table SM2, in SM). Oligomer uptake into the C-S-H gel structure was observed previously by the authors [20], although to a much less significant extent. Variations in the experimental conditions might explain that difference. In the earlier study UCA-T was mixed with a cement paste with a higher portlandite content, favouring the formation of shorter chains (as discussed in Section 3.2.1); and the nominal proportion of consolidant used here was approximately 40% higher (calculated from the data in Table 1), which may have furthered alkoxysilane self-condensation. In addition, the partial carbonation taking place in the gel detected with XRD, FTIR and TG/DTG might have contributed to a decline in the Ca/Si ratio, raising the degree of polymerisation [45].

The oligomeric alkoxysilane interacted differently with C-S-H than with portlandite. The synthesised gel had a Ca/Si ratio >0.8 and <1, a mean chain length of approximately 14 units and an equilibrium pH of

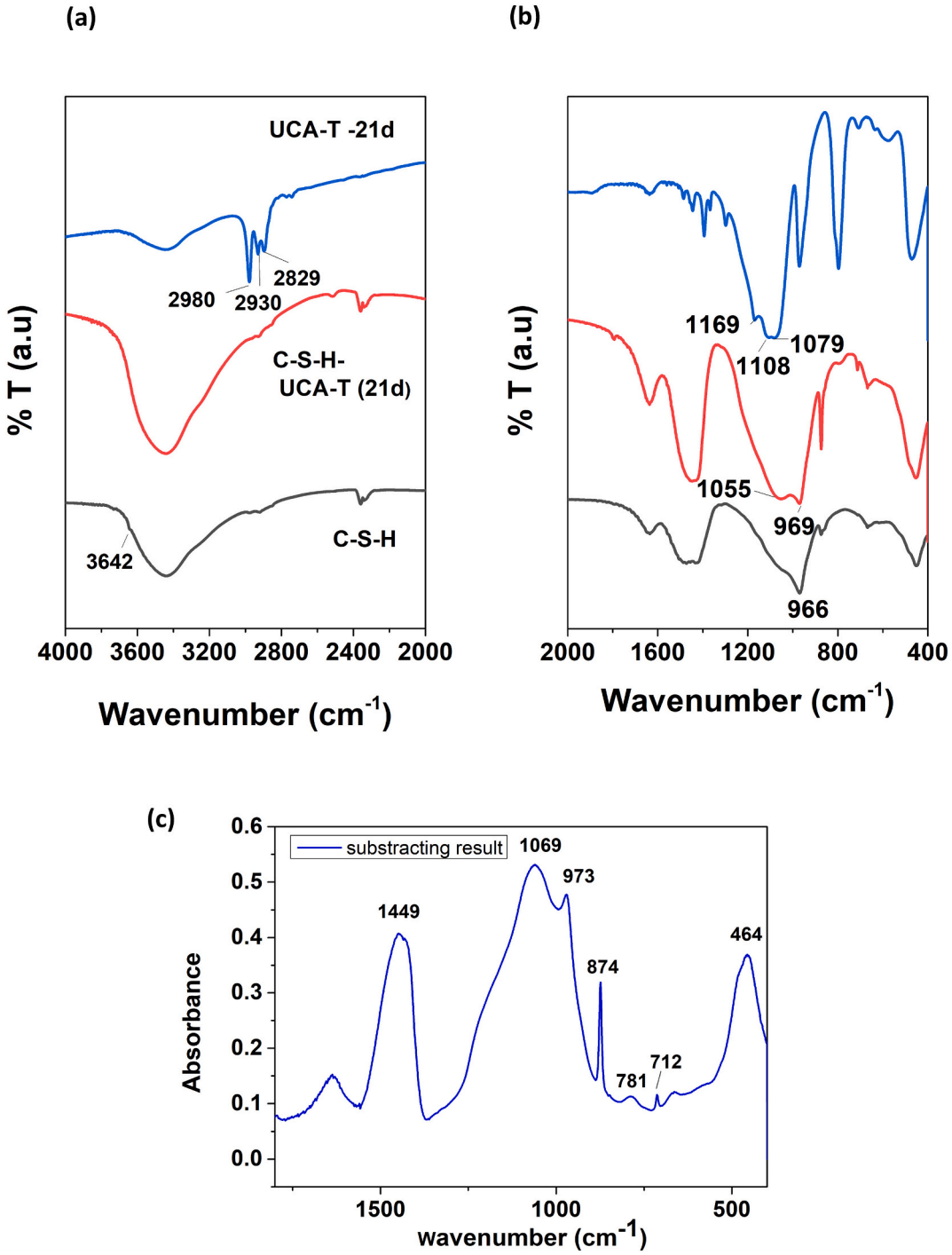

Fig. 7. FTIR spectra for C-S-H, UCA-T-21d and C-S-H-UCA-T-21d; (a) 4000–2000 cm^{-1} region; (b) 2000–400 cm^{-1} region; (c) FTIR findings after subtracting the C-S-H from the C-S-H + UCA-T-21d spectrum.

~11 [46], which although lower than in portlandite (pH ~ 12.472) [32], accelerated hydrolysis, for no organic matter was detected in the 21 d material by TG/DTG or FTIR (the siloxane groups may not have been broken down, however). With the synthetic C-S-H gel, in contrast to the portlandite, two reactions took place: the gel chains were interconnected by hydrolysed monomers, lengthening the MLC to ~44 units, and hydrolysed oligomers condensed to form three-dimensional silica gel structures.

Ayuela et al. [46] showed that in cement hydration the dimeric C-S-H gel structures initially formed are subsequently bridged by a monomer, generating a dreierketten structure. The reasoning is that although synthetic C-S-H gel stimulates UCA-T hydrolysis, its pH would be insufficient to break the siloxane bonds, or at least not quickly enough to prevent the silanols in hydrolysed oligomers from condensing and forming silica gel. The oligomer would interact with synthetic C-S-H gel and lengthen the chain, despite a lower pH and lower [Ca] than in portlandite. The inference is that the gel may act as a seed or template, with the hydrolysed monomers bridging Q^1 units and lengthening the chain. In that case the gel would be highly hydrolysed due to the absence of excess Ca to occupy half of the OH sites in the bridging silica monomers [38].

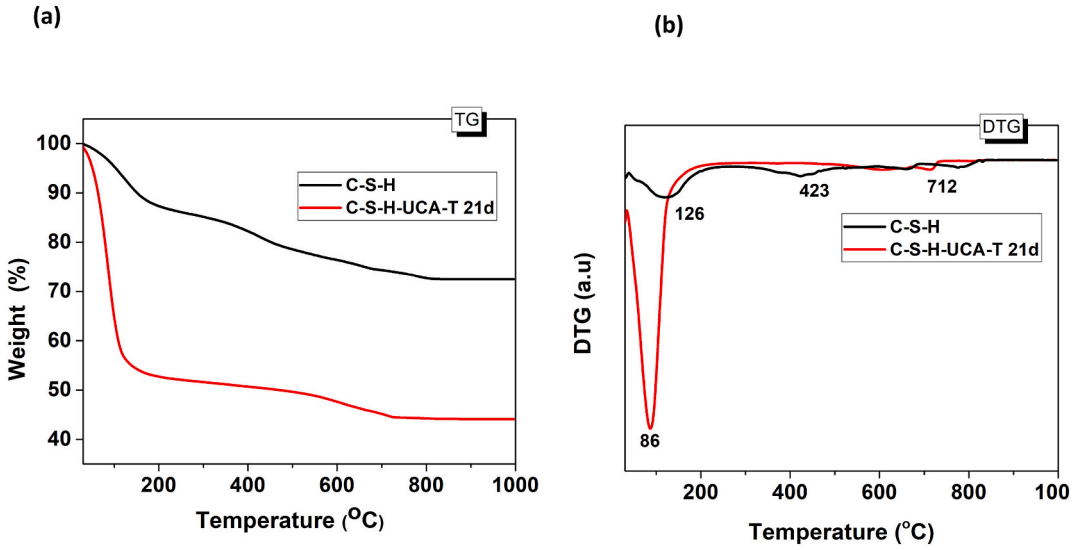

Fig. 8. (a) TG and (b) DTG curves for C-S-H gel and C-S-H-UCA-T-21d.

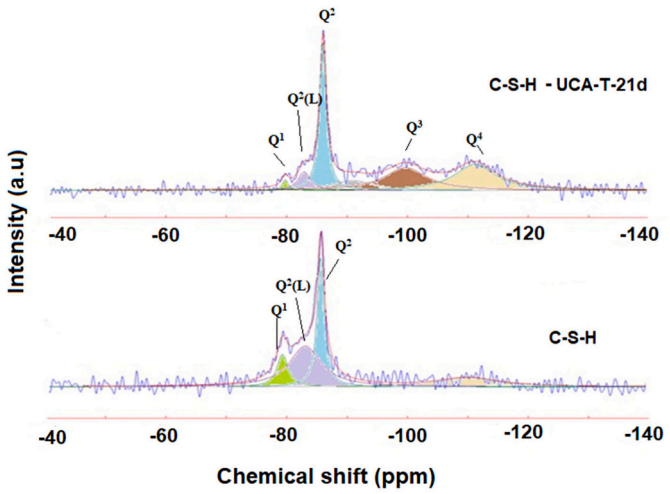

Fig. 9. Deconvoluted ^{29}Si MAS NMR spectra for C-S-H gel and C-S-H-UCA-T-21d.

3.2.3. Interaction between synthetic cement paste (SP) and UCA-T

The diffractograms for the synthetic cement paste (SP) (product of hydrating C_3S with water at 40 C for 1 year) and the same paste after 21 d treatment with UCA-T (SP-UCA-T-21d) are reproduced in Fig. 10(a). The most intense reflections on the original SP diffractogram were assigned to portlandite, while the other wider, less intense lines detected were attributed to C-S-H gel. No reflections for anhydrous C_3S were observed. Certain differences appeared after interaction with UCA-T: the intensity of the portlandite lines declined substantially, C-S-H reflections were still observed and very low intensity calcite lines appeared. The presence of calcite might be the outcome of very minor portlandite carbonation during the process (even though the reactions took place in an N_2 atmosphere) or more probably during the further analysis.

The FTIR spectrum for the original paste (Fig. 10(b)) contained vibration bands typical of the main cement hydration products, portlandite and C-S-H gel [33,34] (SM, Table SM8), as well as carbonate bands at 1474 cm^{-1} and 1421 cm^{-1} [33]. The primary asymmetric band associated with C-S-H gel vibrations housed a shoulder at 922 cm^{-1}, possibly generated by unreacted residual calcium silicate [47].

^{29}Si MAS NMR analysis revealed Q^0 units to account for 5% of the total, denoting the presence of anhydrous C_3S residue. Mean chain length was 3.93 [24].

The FTIR spectrum for the same sample treated with UCA-T exhibited notable differences. A series of very low intensity bands in the 2900 cm^{-1} to 2800 cm^{-1} region, the result of traces of the original UCA-T, denoted incomplete hydrolysis. The intensity of the portlandite band declined substantially, perhaps due to its reaction with UCA-T, although the possibility of minor carbonation cannot be ruled out, an interpretation that would explain the rise in carbonate band intensity (with the band in all likelihood being a combination of the two factors). Although the main Si—O band was not shifted, its asymmetry rose considerably, particularly in the region at >970 cm^{-1}, possibly as the result of an overlap between the main C-S-H gel band and the signal for the residual xerogel formed during UCA-T self-condensation.

The TG/DTG curves for samples SP and SP-UCA-T-21d (synthetic paste + impregnation treatment) are reproduced in Fig. 11. Total mass loss in the original SP came to 20.70% (SM, Table SM9) as a result of the following developments: loss of free or bound water in C-S-H gel (30 °C to 390 °C) [36,37]; portlandite dehydroxylation (390 °C to 510 °C) [36,37]; and amorphous carbonate decarbonation (510 °C to 800 °C) [36,37]. Differences relative to those findings were observed on the TG curves for the synthetic paste bearing UCA-T (SP-UCA-T-21d).The percentage associated with free water or gel water loss rose (in the 30 °C to 125 °C range). The amount of portlandite declined substantially as the carbonate content grew (SM, Table SM9). Signals for the polymerised UCA-T, albeit very small, were still visible (such as the DTG signal at 339 °C in Fig. 11(b)).

In light of the 95% degree of reaction in C_3S determined by NMR and the TG findings and deeming portlandite carbonation to be the source of the carbonates, the Ca/Si ratio in the C-S-H gel in the untreated sample was calculated to be 1.53, a value very close to the 1.67 found by del Bosque et al. for this particular gel [24] using TEM techniques.

The rise in carbonates in the SP-UCA-T-21d sample was an indication that not all the portlandite disappearing from the original paste was carbonated, but rather that part reacted with the hydrolysed oligomers in UCA-T to form C-S-H gel.

Further to the TG results for sample SP-UCA-T-21d, the Ca/Si ratio in the gel in this sample was 1.16. That decline in the Ca/Si ratio implied that the new C-S-H gel formed had a longer chain length than the original phase, a finding consistent with the asymmetry observed for the Si—O asymmetric stretching band on the FTIR spectrum (Fig. 10(b)) and the ^{29}Si MAS NMR results (Fig. 12, Table SM10 (SM)).

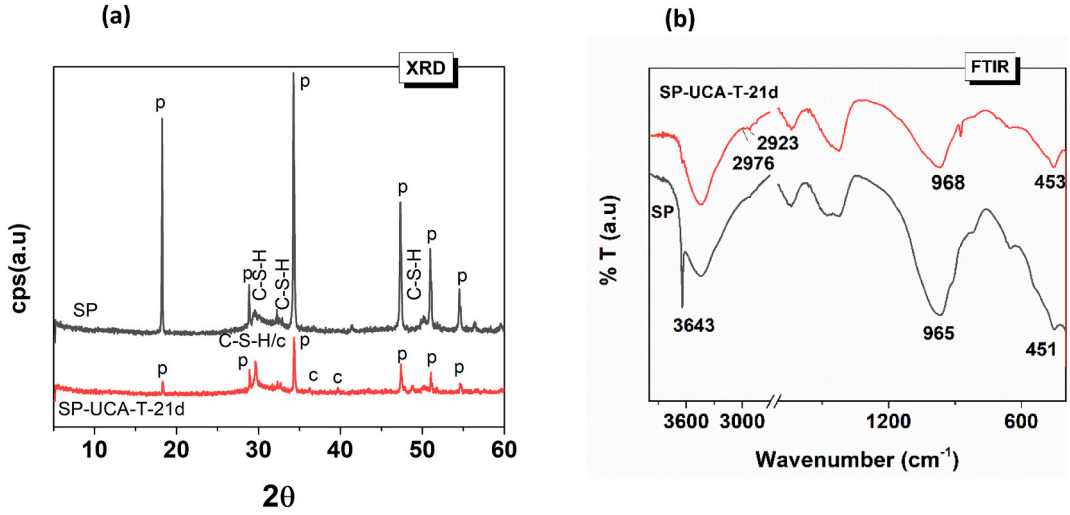

Fig. 10. (a) Diffractograms; and (b) FTIR spectra for samples SP and SP-UCA-T-21d (legend: p, portlandite [$Ca(OH)_2$; (COD 2101033)]; C-S-H, C-S-H gel (COD 9005447); c, calcite (COD 9000095)).

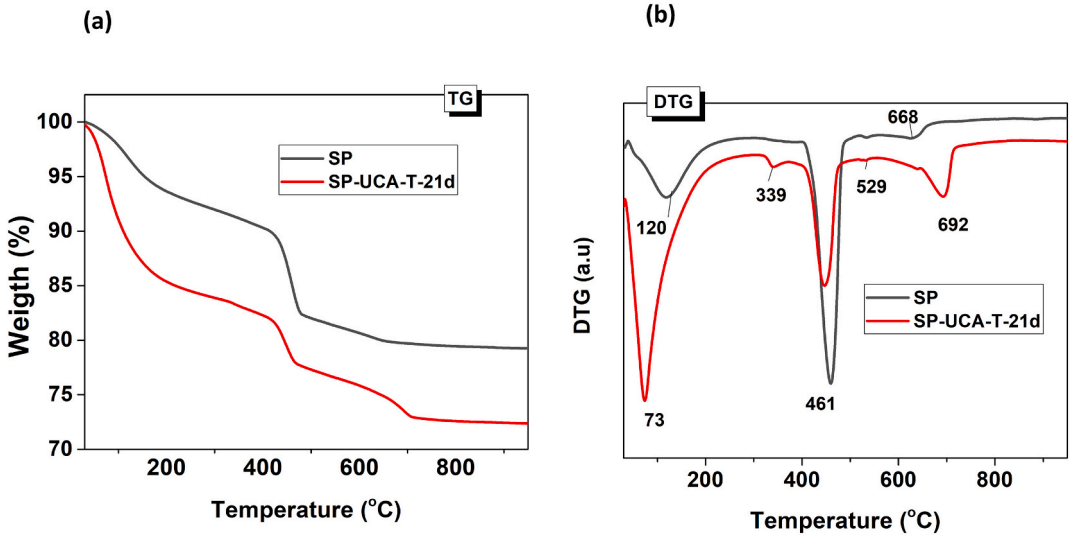

Fig. 11. (a) TG and (b) DTG curves for SP and SP-UCA-T-21d.

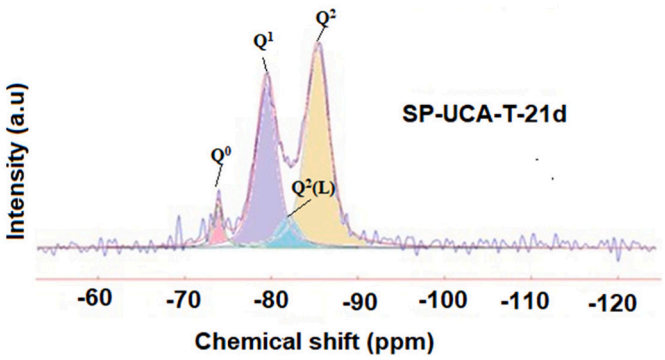

Fig. 12. Deconvoluted ^{29}Si MAS NMR spectrum for SP-UCA-T-21d.

^{29}Si MAS NMR analysis confirmed the presence of units at −79 ppm (Q^1 environments), −82 ppm (Q^2(L)) and −85 ppm (Q^2), structures characteristic of C-S-H gel, as well as an MCL of 5.12 (higher than the 3.93 observed for untreated SP) [21,24]. The increase in mean chain length observed with DTG, FTIR and NMR must have been stimulated not only by high pH, which would break down the oligomeric siloxane groups, but also by the presence of pre-existing C-S-H, that would favour the positioning of monomers on bridging positions. Otherwise, the predominantly dimeric product of the reaction between UCA-T and portlandite, would shorten the MCL and raise the Ca/Si ratio. In that case the C-S-H gel would be less hydroxylated than the synthetic gel described above, given the presence of excess Ca.

3.2.4. Interaction between ettringite (E) and UCA-T

Ettringite ($Ca_6Al_2(SO_4)_3(OH)_{12}{\cdot}26H_2O$) consists in hexagonal, prismatic crystals with a structure characterised by columns of $[Al(OH)_6]$ parallel to axis c, joined by octahedrally coordinated calcium and hydroxyl ions ($[[Ca_6{\cdot}Al_2(OH)_{12}]^{6+}[3SO_4^{2-}{\cdot}26H_2O]^{6-}$) and separated by sulfates and water molecules lying in-in between [48]. At 25 °C, equilibrium pH is 10.36 and the maximum dissolved Ca concentration is 6.31 mmol/kg, whereas at pH of over 11 [Ca] is less than 1 mmol/kg and the solubility product is $\log_{10}K_{sp} = -44.91$ ($Ca_6[Al(OH)_6]_2(SO_4)_3{\cdot}26H_2O = 6Ca^{2+} + 2Al(OH)^-_4 + 3SO_4^{2-} + 4OH^- + 26H_2O$) [49,50]. The diffractogram in Fig. 13(a) for ettringite (ET) shows a predominance of that mineral, along with reflections for

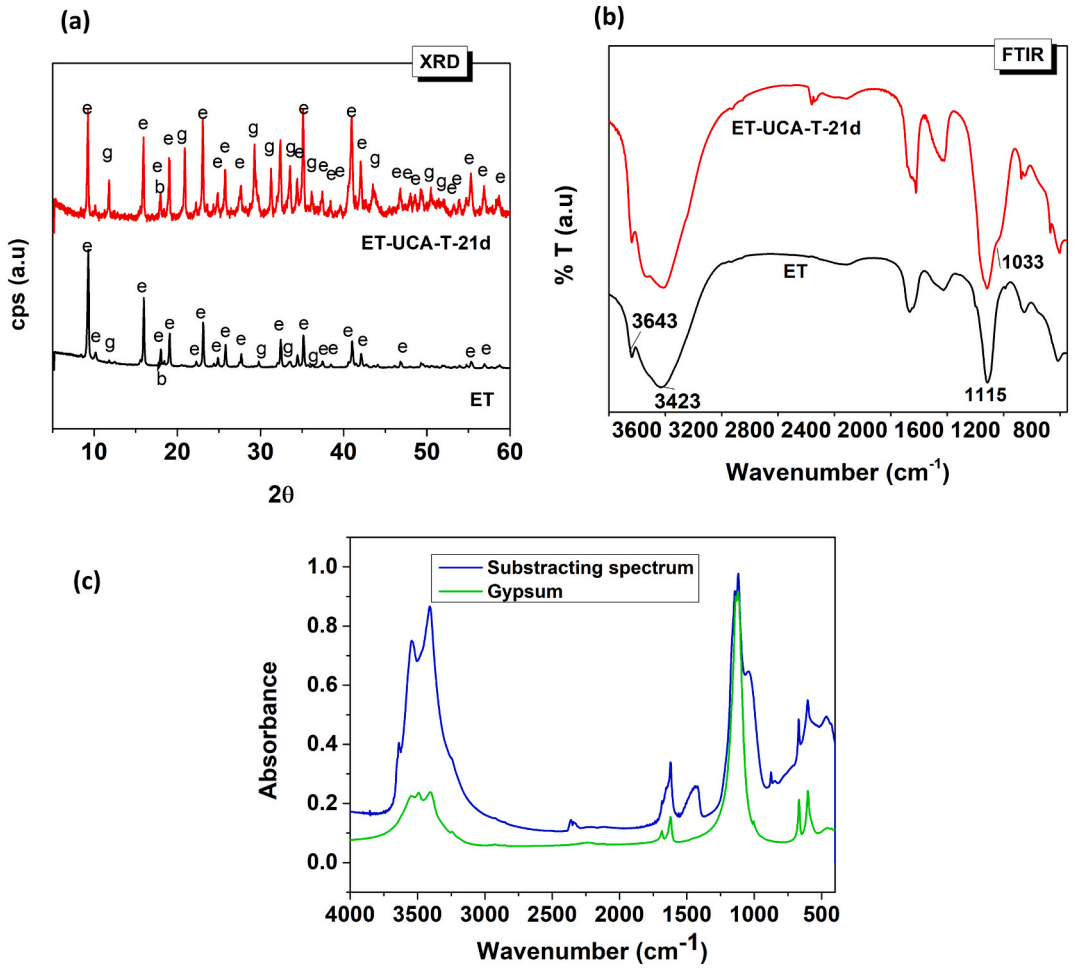

Fig. 13. (a) Diffractogram for the original ettringite (ET) and ettringite with the consolidant (ET-UCA-T-21d) (legend: e, ettringite (COD 90103); b, gypsum (COD 2300259); g, gibbsite (COD 9003864); c, calcite (COD 9016705)); (b) FTIR for samples ET and ET-UCA-T-21d; (c) FTIR spectrum resulting from subtracting spectrum ET from spectrum ET + UCA-T-21d.

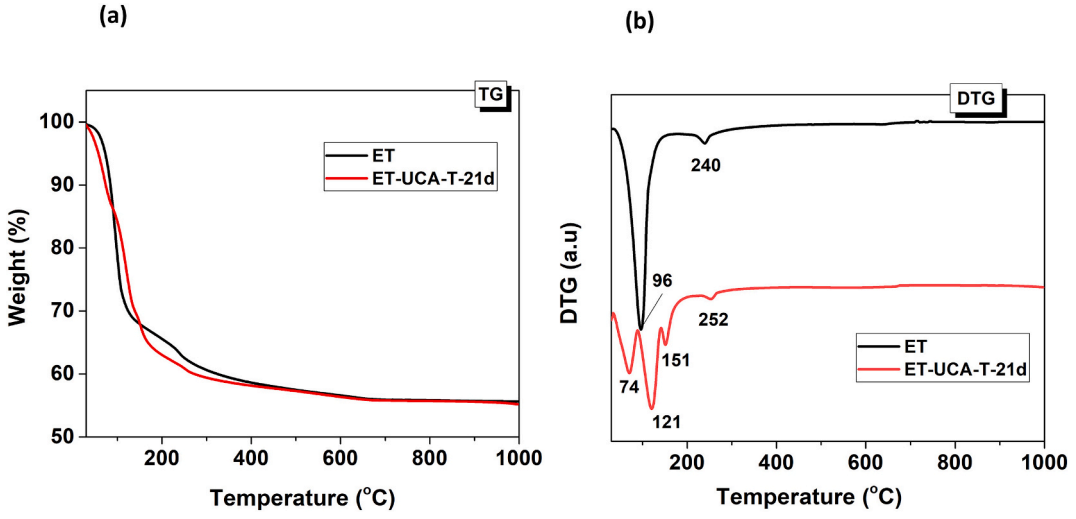

Fig. 14. (a) TG and (b) DTG curves for ET and ET-UCA-T-21d.

gypsum and gibbsite. Rietveld quantitative analysis of the ettringite phase revealed 98.66% purity for the product synthesised (JCPDS, PDF 72-0646), the rest up to 100% consisting in a mix of gypsum (JCPDS, PDF 33-0311) and gibbsite (wRp = 8.60%).

The XRD pattern for ET-UCA-T-21d (Fig. 13(a)) also contained ettringite reflections and lines attributed to gypsum (much more intense than on the pattern for the original ettringite), possibly implying that the alkoxysilane partially decomposed part of the ettringite to gypsum.

Ettringite, like the other phases studied, stimulated UCA-T oligomer hydrolysis; after 21 d of treatment no bands characteristic of ethoxy groups were observed on the FTIR spectrum. Treatment modified the ettringite FTIR spectrum (Fig. 13(b)). A new band appeared at 3525 cm^{-1} in the O—H stretching vibration region (SM, Table SM11), while the primary band shifted to 3412 cm^{-1}. A new band also appeared in the 1700 cm^{-1} to 1600 cm^{-1} region associated with bending vibrations in water, at around 1621 cm^{-1}, attributable to gypsum [33,51]. Wide carbonate bands were observed in the 1400 cm^{-1} to 1500 cm^{-1} asymmetric stretching region, along with bending bands at around 875 cm^{-1} attributed to C—O vibrations in carbonates and 850 cm^{-1} to Al—O vibrations in ettringite [39], as well as two new bands at 669 cm^{-1} and 604 cm^{-1}, characteristic of gypsum [33,51].

Subtracting the ET from the ET-UCA-T-21d spectrum yielded a spectrum similar to that for gypsum, although with an extra band at around 1033 cm^{-1} not attributable to S—O vibrations in sulfates (Fig. 13(c)). That band might have been generated by Si—O vibrations [35] possibly associated with a product of the reaction between the consolidant and ettringite.

The TG curves for the aforementioned samples are reproduced in Fig. 14(a) and the DTG curves in Fig. 14(b). Although percentage mass loss in the original ET, at ~44%, was about the same as in the sample treated with the consolidant for 21 d (ET-UCA-T-21d) (Fig. 14(a); Table SM12 in SM), the curves varied, particularly in the 30 °C to 350 °C region. The DTG curve for the original ET (Fig. 14(b)) exhibited a predominant peak at around 96 °C and a lower intensity signal at 240 °C associated with the loss of bound water with different bond energies [26]. The latter would have been generated by dehydroxylation of the $Al(OH)_3$ [52], a phase detected by Rietveld analysis of the XRD findings.

The post-treatment DTG curve differed substantially from the curve for the original ettringite. Three intense peaks were observed, at 74 °C, 121 °C and 151 °C, the first probably due to residual free water or water in ettringite [53] and the latter two perhaps to water loss from gypsum ($(CaSO_4{\cdot}2H_2O) \rightarrow$ hemihydrate ($CaSO_4{\cdot}1/2H_2O$) $\rightarrow$ anhydrite ($CaSO_4$)) [36,52], a phase identified with XRD (Fig. 14(a)). The signal for $Al(OH)_3$ was shifted to a slightly higher temperature, 252 °C, on the ET-UCA-T-21d curve.

The literature normally associates ettringite decomposition to gypsum with carbonation, further to a reaction simplified as shown in Eq. (5):

$$3CaO{\cdot}Al_2O_3{\cdot}3CaSO_4{\cdot}32H_2O + 3CO_2 \rightarrow 3CaSO_4{\cdot}2H_2O + 3CaCO_3 + 2Al(OH)_3 + 23\ H_2O \quad (5)$$

Ettringite is extraordinarily sensitive to the presence of CO_2, particularly in moist environments [54,55]. Nonetheless, the diffractogram contained no reflections for calcite or any other $CaCO_3$ polymorph, nor was any significant carbonation observed in the FTIR or TG/DTG analyses. Ettringite decomposition must consequently have been driven by the alkoxysilane applied.

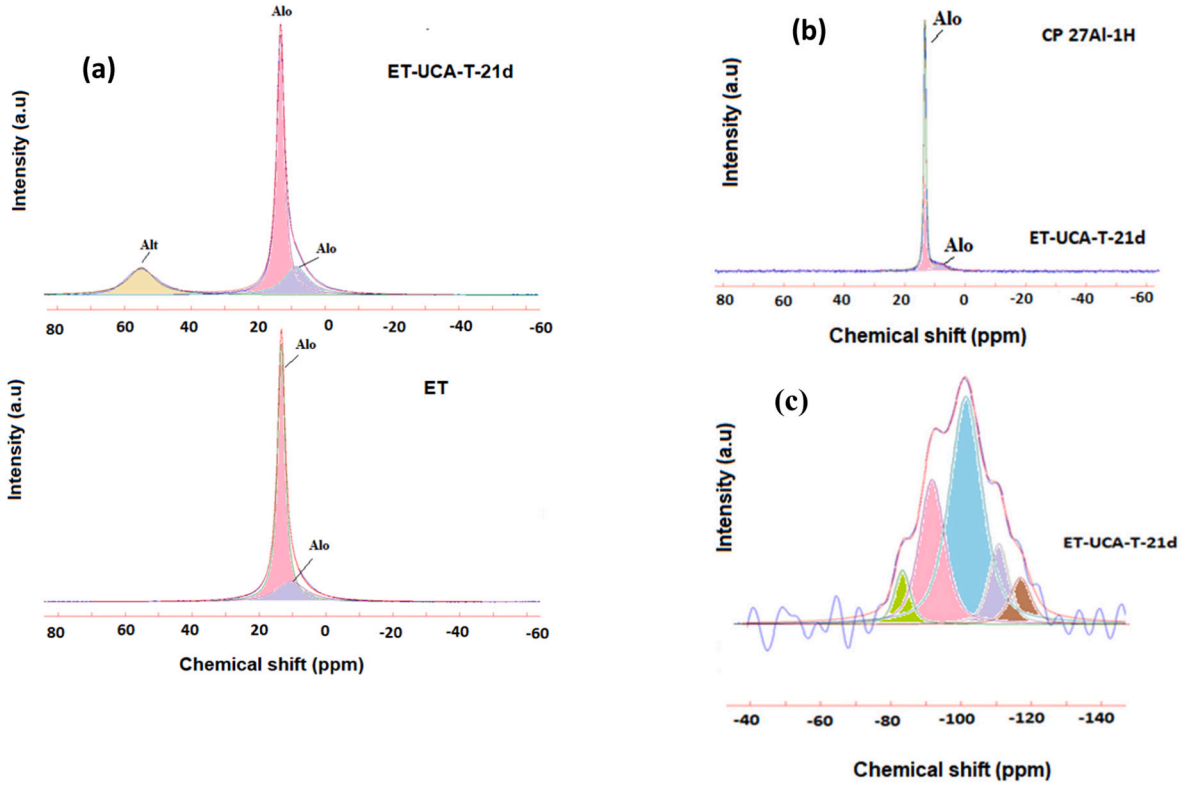

Fig. 15. Deconvoluted (a) ^{27}Al MAS NMR; (b) CP ^{27}Al-^{1}H; and (c) ^{29}Si MAS NMR spectra for samples ET and ET + UCA-T-21d (components obtained after the deconvolution process, could be assigned to $Q^3(nAl)$ or $Q^4(nAl)$ units).

$$3CaO{\cdot}Al_2O_3{\cdot}3CaSO_4{\cdot}32H_2O + xSi(OH)_4 \rightarrow 3CaSO_4{\cdot}2H_2O + (CaO)z.(Al_2O_3)y.(SiO_2)x.(H_2O)q + (2-y)Al(OH)_3 + (23+2x-q-3/2y)H_2O \quad (6)$$

Further information on the product formed was sought with ^{29}Si and ^{27}Al MAS NMR analysis of sample ET-UCA-T-21d. Fig. 15(a) reproduces the deconvoluted spectrum for ^{27}Al MAS NMR for ET and ET-UCA-T-21d and Fig. 15(c) the deconvoluted ^{29}Si MAS NMR spectrum for ET-UCA-T-21d.

The ^{27}Al spectrum for the original ettringite exhibited a very intense signal at +13.27 ppm attributable to the octahedral Al in ettringite [56,57] and a much smaller signal at +10.4 ppm to residual gibbsite [56], likewise detected by XRD. After treatment with UCA-T the ^{27}Al spectrum changed: in addition to the ettringite signal at +13.27 ppm, the area of the gibbsite Al_O signal at +10.4 ppm rose from around 19% in sample ET to 26% in sample ET-UCA-T-21d, confirming the possible decomposition of ettringite as per Eq. (6). The most significant feature, however, was the appearance of a new signal in the tetrahedral Al region, at +54.89 ppm, typical of the Al_T in aluminosilicates [43]. The silica oligomers resulting from consolidant hydrolysis would react with the aluminium from ettringite decomposition to form an amorphous aluminosilicate gel. The FTIR vibration band observed at around 1030 cm^{-1} to 1040 cm^{-1}, typical of Si—O bonds in aluminosilicates [35], may support that hypothesis.

The CP ^1H-^{27}Al spectrum for Al in this sample (Fig. 15(b)) showed that the Al_T component practically disappeared, confirming that this Al would be coordinated with silicon species (Si-O-Al bonds) rather than with OH groups.

The ^{29}Si MAS spectrum for sample ET-UCA-T-21d in Fig. 15(c) contained a very wide asymmetric signal between −80 ppm and −120 ppm, substantially different to the one generated by UCA-T-21d (Fig. 2). The signal-to-noise ratio is lower than in the previous ^{29}Si MAS NMR spectra (due to the small number of active ^{29}Si isotopes), however a tentative deconvolution of that signal revealed the presence of components which, depending on their position, might be assigned to Q^3(nAl) or Q^4(nAl) environments (SM, Table SM13). The presence of silica environments different to those of the polymerised consolidant (Fig. 2) confirmed that the UCA-T oligomers reacted with the aluminium present in ettringite to form some manner of amorphous flat or three-dimensionally structured aluminosilicate. Those gels would differ substantially from the ones generated in the $Ca(OH)_2$-UCA-T-21d reaction, which bear a closer resemblance to C-S-H-like gels (linear chain structures). As ettringite decomposition yields gypsum, the Ca from the sulfate would not be available to react with $Si(OH)_4$, which would, rather, react and condense with the $Al(OH)_6$ in ettringite, taking the Al up in tetrahedral positions and compensating the charge with 1/3 of the Ca available ($2Al^{3+} + Ca^{2+} \Leftrightarrow 2Si^{4+}$).

The CP-^1H-^{29}Si spectrum contained no signal, confirming that the silicates were coordinated in aluminium environments rather than with OH groups. That suggests that the valence imbalance stemming from the replacement of Si^{4+} with Al^{3+} would have to be offset with the Ca^{2+} resulting from ettringite decomposition ($Ca^{2+} + 2Al^{3+} \rightarrow 2Si^{4+}$).

These results contrast with earlier findings according to which decomposition of the ettringite present in a portland cement due to its reaction with the impregnation treatment was not initially observed [20]. The apparent discrepancy might be explained by the fact that under the conditions prevailing in that study, UCA-T would react predominantly with other phases such as portlandite and C-S-H.

3.2.5. *Interaction between monocarboaluminate (MC) and UCA-T*

Calcium monocarboaluminate hydrate $3CaO{\cdot}Al_2O_3{\cdot}CaCO_3{\cdot}11H_2O$ (MC) forms part of a family of laminar compounds generically known as AFm phases. It crystallises in the triclinic system with a structure consisting in interlayered aluminates $[Ca_4Al_2(OH)_{12}]^{2+}$, water and carbonates ($(2H_2O)$–$(CO_3)^{2+}{\cdot}3H2O$) [58]. Its 25 °C equilibrium pH is 11.67, its solubility product ($log_{10}K_{sp}$) is 31.12 and calcium solubility under those conditions is 3.73 mmol/l (solubility calculated assuming 84 d calcite saturation in the supernatant and the dissolution reaction to be: $Ca_4Al_2(CO_3)(OH)_{12}{\cdot}5H_2O \rightarrow 4Ca^{2+} + 2AlO - 2 + CO_3^{2-} + 4OH^- + 9H_2O$) [59].

The diffractograms for the original monocarboaluminate (MC) and the same sample after interacting for 21 d with UCA-T (MC-UCA-T-21d) are reproduced in Fig. 16(a). In addition to the typical MC ($Ca_4Al_2(CO_3)(OH)_{12}{\cdot}5H_2O$) signal, the XRD pattern for the original phase contained reflections for residual C_3A and calcite ($CaCO_3$), as well as a series of signals associated with gibbsite ($Al(OH)_3$). Low intensity reflections

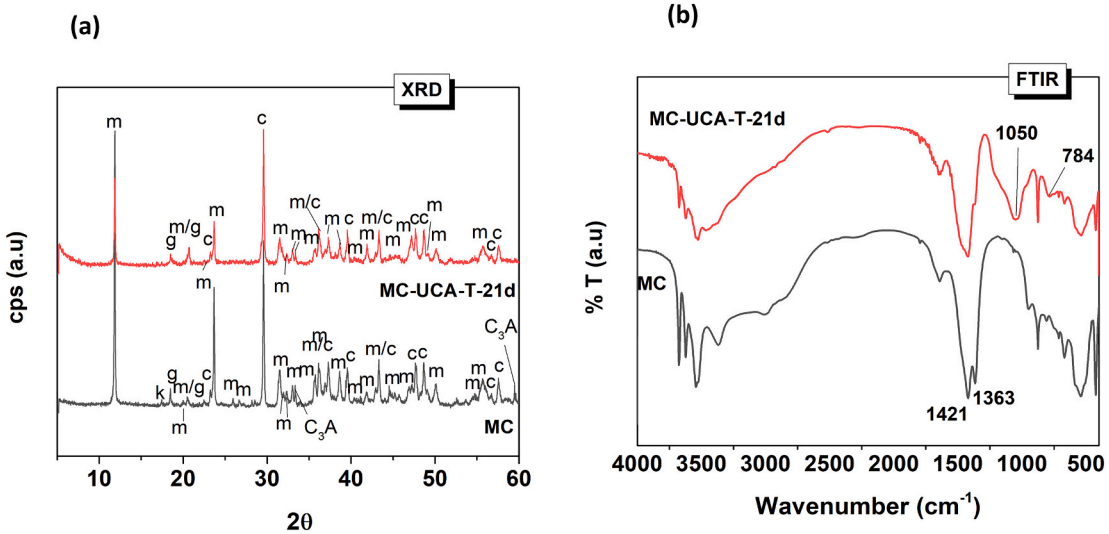

Fig. 16. (a) Diffractograms (legend: m, monocarboaluminate (COD 2007668); g, gibbsite (COD 1011081); C_3A, tricalcium aluminate (COD 9015966); c, calcite (COD 9000095); k, katoite (COD 9005159)); and (b) FTIR spectra for samples MC and MC-UCA-T-21d.

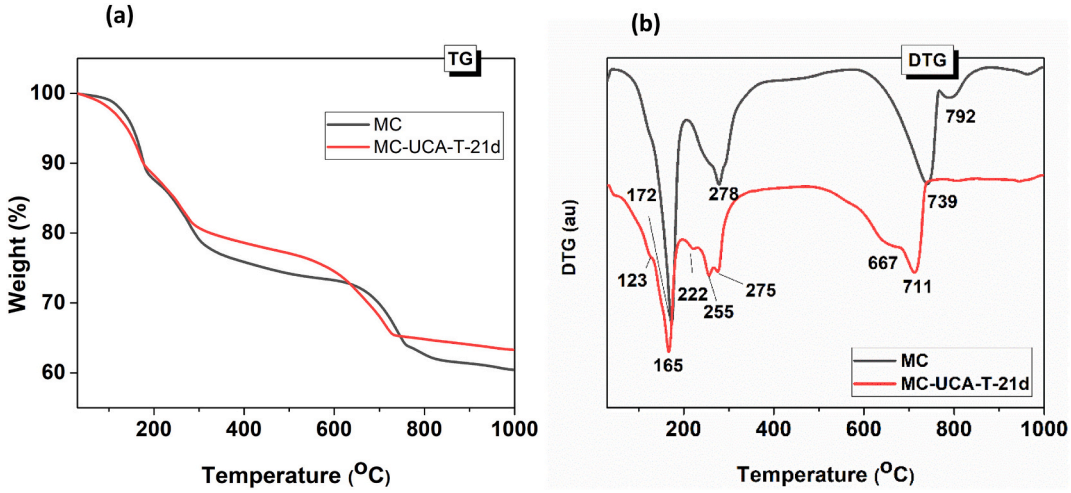

Fig. 17. (a) TG and (b) DTG curves for MC and MC-UCA-T-21d.

associated with katoite ($Ca_3Al_2H_{12}O_{12}$) were also present.

The FTIR spectrum (Fig. 16(b)) for the sample treated with UCA-T shows no trace of ethoxy groups, further confirming that this phase accelerated the alkoxysilane hydrolysis, aside from clear modifications of the original sample and evidences of minor monocarboaluminate decomposition. Intensity declined and relative intensity was altered in the bands in the 3700 cm^{-1} to 3500 cm^{-1} region, associated with the various types of O—H vibrations in the OH groups in $Ca_4Al_2(CO_3)(OH)_{12}{\cdot}5H_2O$ (MC) (SM, Table SM14). The new band at 3465 cm^{-1} and its shoulders at 3397 cm^{-1} and 3376 cm^{-1} were compatible with the absorptions that would be induced by gibbsite if present [33]. Lower intensity was also found for the band at 1363 cm^{-1}, attributed to C—O vibrations in MC [60], while the broadening toward higher wavenumbers in the signal at 1425 cm^{-1} denoted partial monocarboaluminate decomposition and precipitation of an amorphous carbonate and gibbsite. In addition, the spectrum for MC-UCA-T-21d contained a new, very wide asymmetric signal in the silicate vibration region centred at 1050 cm^{-1}, i.e., shifted toward significantly lower frequencies than the 1080 cm^{-1} observed for the polymerised UCA-T (SM, Table SM1). That signal overlapped partially with the band at 1020 cm^{-1} indicative of the gibbsite (or $Al(OH)_3\ nH_2O$) generated as a result of partial MC decomposition. As in the preceding cases, such a substantial shift may denote a reaction between the alkoxysilane oligomers and MC, yielding an aluminosilicate gel (aluminium uptake in silica gels shifts the signal to lower frequencies).

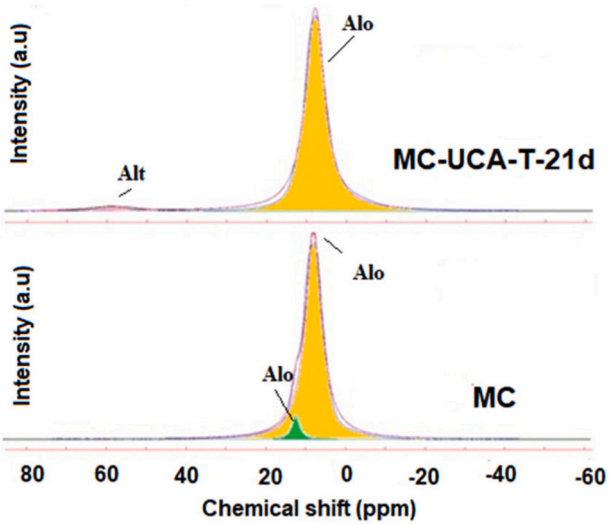

Fig. 18. ^{27}Al MAS NMR spectra for MC and MC-UCA-T-21d.

The TG/DTG curves for the two samples reproduced in Fig. 17 exhibit obvious differences. The DTG curve for the original monocarboaluminate contained two peaks at 172 °C and 278 °C, a sign of two-stage MC dehydration [52,61], in which an initial loss of the five interlayer water molecules was followed by the loss of six water molecules in the octahedral layer. Both signals tend to appear as double bands [61], visible here as shoulders at 125 °C on the 172 °C peak and 257 °C on the 278 °C peak. The latter exhibited a second shoulder at 291 °C, attributed to katoite. The other two other peaks observed, at 739 °C and 792 °C, identified calcite and MC decarbonation, respectively [61].

The peaks at 172 °C and 278 °C on the curve for the original sample were shifted to slightly lower temperatures (165 °C and 275 °C, respectively) on the DTG curve for sample MC-UCAT-21-d. A new shoulder appeared at 222 °C, whereas the one assigned to katoite was no longer visible. All these bands might also be assigned to MC dehydration [61]. The most significant change, however, was found in the DTG peak associated with carbonate decomposition, which widened considerably and shifted from 739 °C to 711 °C with a shoulder at 667 °C, the result of the overlap between the CO_2 losses in calcite and in MC.

The total mass loss in the two samples above 450 °C was an identical 14.51%, indicating that whereas the oligomer partially decomposed monocarboaluminate to yield a very amorphous calcium carbonate, the sample was not carbonated.

The ^{27}Al spectra for the original monocarboaluminate and the phase after reacting for 21 d with the impregnation treatment are reproduced in Fig. 18. The original MC exhibited an intense signal at around +8 ppm attributed to Al_O (probably overlapping with the Al_O in the small amount of gibbsite detected with XRD). Similarly, a small shoulder observed at +12.4 ppm was assigned to the Al_O in the katoite identified as a secondary phase in XRD analysis. The post-treatment spectrum contained a new very intense signal (96% of the area) at +8.1 ppm attributed to the Al_O in MC, along with a low intensity, barely perceptible signal at +56 ppm in the tetrahedral aluminium region (4% of the area). That tetrahedral aluminium signal suggested that an Al_T able to react with the silica present in the UCA-T was generated during partial MC decomposition. The intense signal at +8.1 ppm would overlap with the signal for the gibbsite identified with XRD, TG and FTIR.

The ^{29}Si NMR spectrum for MC-UCA-T-21d could not be readily interpreted due to the low signal-to-noise ratio. In contrast with the previously discussed phases, all the silicon in the sample is sourced from the UCA-T and, in conjunction with a lower proportion of product (see Table 1) and ^{29}Si active nuclei, would generate this type of spectra. As a

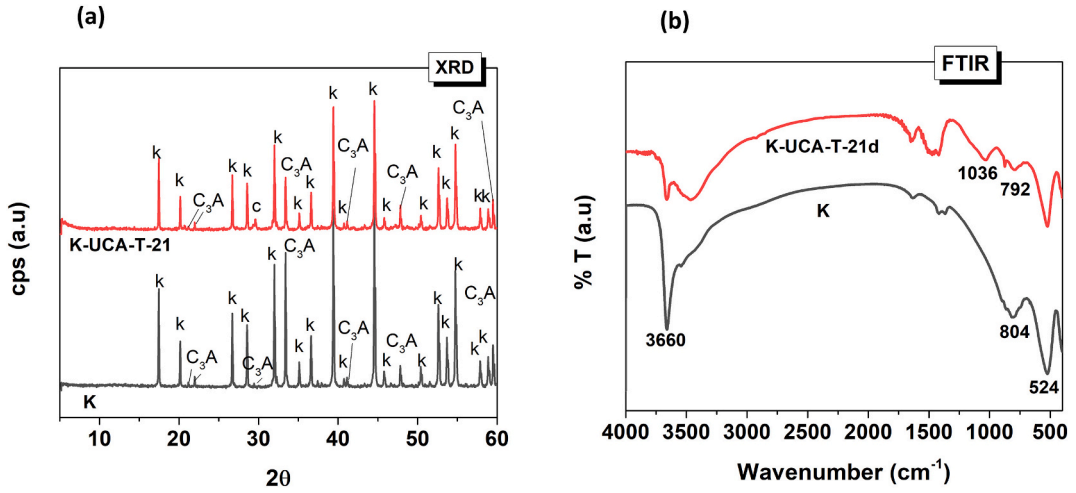

Fig. 19. (a) Diffractograms and (b) FTIR spectra for K and K-UCA-T-21d (legend: K, katoite (COD 9001085); C_3A, tricalcium aluminate (COD 9015966)).

result, no analysis was possible under the present recording conditions.

The small Al_T signal on the ^{27}Al MAS NMR spectrum, together with the FTIR band at 1050 cm^{-1}, might suggest the formation of a silicon-based gel able to take Al up into its composition. The breadth of the main signal on the FTIR band, centred at 1050 cm^{-1}, would be an indication that the band was the result of the sum of several components: signals attributable to residual silica in UCA-T that might take up aluminium in tetrahedral environments and Al—O vibrations in the gibbsite (or alumina gel) generated as a result of partial decomposition.

3.2.6. *Interaction between katoite (K) and UCA-T*

Katoite crystallises in the cubic system with structure comprising a three-dimensional system of octahedral [$Al(OH)_6$] and dodecahedral [$Ca(OH)_8$] [61] units. At 25 °C (84 d) its solubility product ($\log_{10}K_{sp}$) is −20.84, its Ca concentration 6.31 mmol/l and its pH 11.81 (dissolution reaction $Ca_3Al_2(OH)_{12} \rightarrow 3Ca^{2+} + 2AlO - 2 + 4OH^- + 4H_2O$) [59].

The diffractograms for the original katoite (K) and the phase with the impregnation treatment (K-UCA-T-21d) are reproduced in Fig. 19(a). In addition to the reflections characteristic of the mineral (k: $C_3Al_2(OH)_{12}$), the XRD pattern for katoite contained a series of lines associated with the C_3A from which it was synthesised. Adding UCA-T induced a decline in C_3A reflection intensity, probably a result of phase hydration, favoured by the high relative humidity. The intensity of the katoite peaks was barely affected (outside of a slight decline). A low intensity signal at 2θ 29° attributable to slight carbonation (despite the controlled N_2 working atmosphere) was detected.

The FTIR spectrum for the original katoite (K) (Fig. 19(b)) exhibited a band at 3660 cm^{-1} (SM, Table SM15) characteristic of O—H vibrations in the katoite OH groups and bands at 804 cm^{-1} and 524 cm^{-1} induced by Al—O vibrations [62]. The spectrum for sample K-UCA-T-21d, which contained no ethoxy group bands, differed from the spectrum for K. The intensity of the band at 3660 cm^{-1} declined and new bands appeared at 3470 cm^{-1}, indicative of O—H stretching, and at 1645 cm^{-1}, of bending vibrations in water. The carbonate bands at 1425 cm^{-1} grew slightly [35] and others typical of Si—O vibrations arose at around 1036 cm^{-1} (wide and asymmetric) and 792 cm^{-1}. The latter was also present in the polymerised UCA-T (SM, Table SM2). The wide breadth of the main band (centre of gravity at 1030 cm^{-1}) was probably due to overlapping between residual alkoxysilane units and a silicon-high gel formed as a result of its polymerisation.

Katoite lost water at temperatures of 25 °C to 100 °C (Fig. 20), although with only a 1.2% mass loss up to 200 °C and 0.98% at >600 °C. The overall loss was 24.35%. The DTG curve (Fig. 20(b)) showed two endothermal signals, one very intense at 300 °C and weaker second peak at 437 °C attributed to the loss of hydroxyl groups octahedrally coordinated with the Al in the katoite structure [63]. An exothermal signal denoting the reaction of the oxides CaO and Al_2O_3 generated in thermal treatment was observed at around 890 °C. Based on the mass losses and

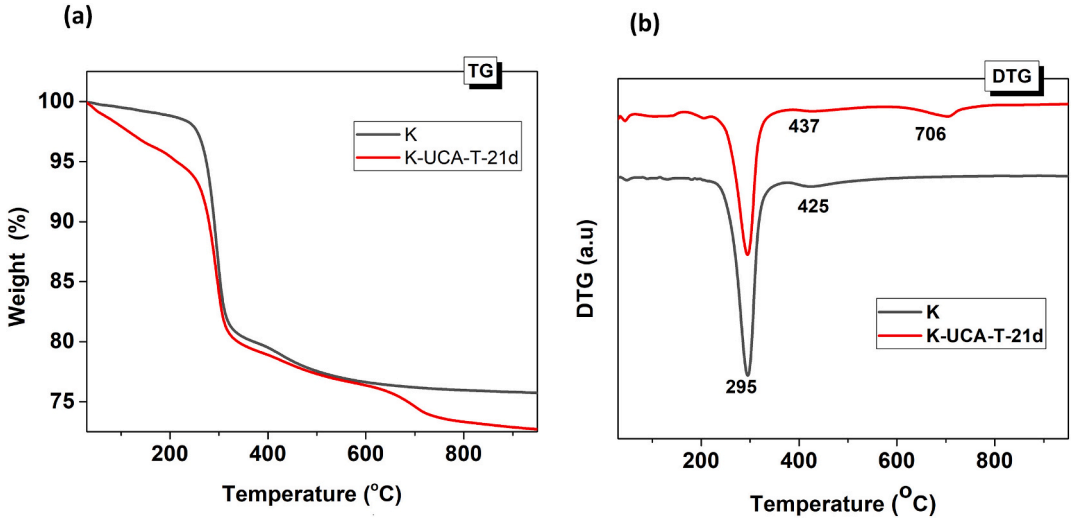

Fig. 20. (a) TG and (b) DTG curves for K and K-UCA-T-21d.

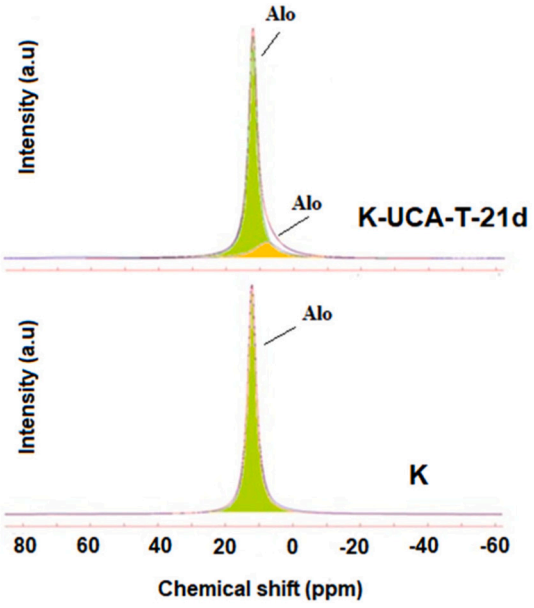

Fig. 21. ^{27}Al MAS NMR spectra for K and K-UCA-T-21d.

the residue remaining after thermal analysis, the sample was determined to contain 81% katoite and 17% anhydrous C_3A.

The TG curve for sample K-UCA-T-21d (Fig. 20(a)) contained the same peaks as the untreated phase, although at lower intensity, as well as an endothermal decline in mass from 25 °C to 200 °C due to weakly bound water loss in the katoite - alkoxysilane reaction products. A new endothermal peak at 700 °C was assigned to the thermal decomposition of the carbonates more than likely generated [42,63] by sample weathering during handling.

The 5.3% mass loss from 25 °C to 225 °C as determined by TG was attributed to the loss of hygroscopic water or water bound to the alumina generated during katoite decomposition; the 18.3% loss up to 600 °C to katoite dehydroxylation; a further 3.03% was associated with CO_2 loss and 0.7% with loss of the water released in the exothermal oxide reaction.

In light of the mass loss findings, analysis of the dry residue after TG, the proportion of katoite and UCA-T in the sample (Table 1) and assuming a 60% total mass loss in the fully hydrolysed UCA-T, the composition of the K-UCA-T-21d sample was calculated as: 63.0% katoite, 14% C_3A, 6.8% $CaCO_3$ and 7.5% SiO_2. On those grounds, approximately 12% of the katoite was estimated to have been decomposed by reaction with the alkoxysilane.

^{27}Al NMR analysis was conducted to determine the changes in katoite nanostructure as a result of its interaction with the impregnation treatment. The spectra for the substrate before and after interaction with the consolidant are reproduced in Fig. 21. Both contained a signal at +12 ppm assigned to the Al_O in katoite, although none was observed for Al_T (in contrast to MC) [64], perhaps suggesting that in this case Al was not taken up into the siliceous gel. The signal normally appearing at +75.9 ppm and characteristic of C_3A [56] was likewise absent, probably for reasons of dilution, for the amount of Al_O in the sample was vastly greater than the Al_T sourced from the C_3A. In addition to the component at +12 ppm associated with katoite, the deconvoluted spectrum for sample K-UCA-T-21d exhibited a smaller component located at lower chemical shifts (~+8 ppm) which, based on its position, might constitute some manner of amorphous carboaluminate not detectable with XRD.

As in the case of monocarboaluminate, ^{29}Si analysis of katoite was hindered by the small number of active ^{29}Si isotopes in the sample and the concomitantly low signal-to-noise ratio that rendered suitable assignment of the silicon environments impossible. This point would need to be addressed in a future research.

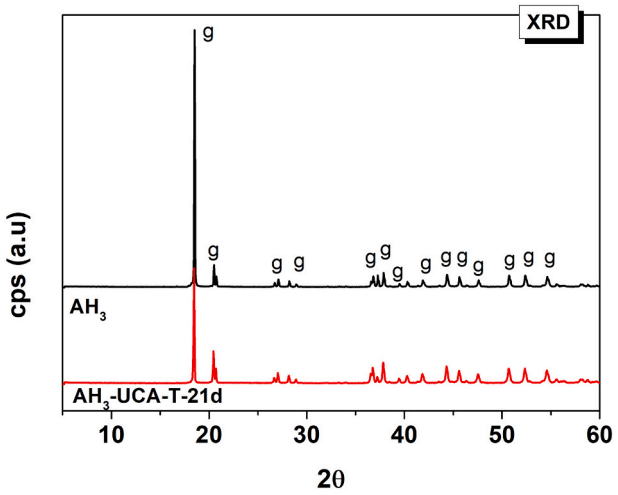

Fig. 22. Diffractograms for AH_3 and AH_3-UCA-T-21d (legend: g, gibbsite (COD 1011081)).

3.2.7. *Interaction between gibbsite (AH_3) and UCA-T*

Gibbsite ($Al(OH)_3$), which crystallises in the monoclinic system, may exhibit small tabular habits with pseudohexagonal and prismatic edges or form lamellar or stalactite-like clusters. Its structure consists in a single layer of Al ions sandwiched between two of hexagonally packed hydroxyl ions. The Al interlayers comprise octahedra joined at the edges, with only two of every three housing an Al^{3+} in the centre, which is coordinated with hydroxyl ions [65]. Its equilibrium pH is 6.99 and its solubility product ($\log_{10}K_{sp}$) 7.23 for the dissociation reaction $Al(OH)_3 + 3H^+ = Al^{3+} + 3H_2O$ [32].

The diffractograms for the AH_3 substrate and the same sample after interacting for 21 d with UCA-T (AH_3-UCA-T-21d) are reproduced in Fig. 22. The reflections characteristic of gibbsite were the only lines on the patterns, where no other phases were detected.

The FTIR spectra for the original gibbsite (AH_3) and the post-treatment substrate (AH_3-UCA-T-21d) (SM, Table SM16) are reproduced in Fig. 23. The spectrum for the former exhibited bands assigned to the various types of OH and Al—O vibrations in AH_3 [66]. After treatment with the consolidant the most significant differences were the presence of C—H vibrations generated by the Et groups in UCA-T and the wide symmetric vibration band located at wavenumbers in the 1000 cm^{-1} to 1300 cm^{-1} region. Assigned to different types of Si—O vibrations, that band had a shoulder at 1085 cm^{-1}, also detected in the polymerised UCA-T. Its detection, along with the presence of ethoxy group vibration bands, denoted incomplete product hydrolysis, for the FTIR spectrum identified a combination of polymerised but not fully hydrolysed UCA-T and gibbsite.

The TG/DTG curves for the samples are reproduced in Fig. 24. Total mass loss was practically identical in the two, at 34.62%, and matched the stoichiometric loss associated with $Al(OH)_3$ dehydroxylation. The DTG curves were also very similar, with three signals at 237 °C, 302 °C and 524 °C. Synthetic gibbsite (such as the laboratory reagent used here) decomposition consists in three partial reactions. At 200 °C to 230 °C $Al(OH)_3$ dehydroxylates to γ-AlOOH (deficient bohemite); at 270 °C to 240 °C it dehydroxylates to λ-Al_2O_3; and at 500 °C to 540 °C γ-AlOOH dehydroxylates to λ-Al_2O_3.

Gibbsite would consequently appear to be stable in the presence of the impregnation treatment, for no chemical interaction between the two was detected. Analysis of the interaction products revealed the presence of unaltered gibbsite and residual polymerised UCA-T. The pH of this phase was not, then, sufficiently alkaline to favour UCA-T hydrolysis.

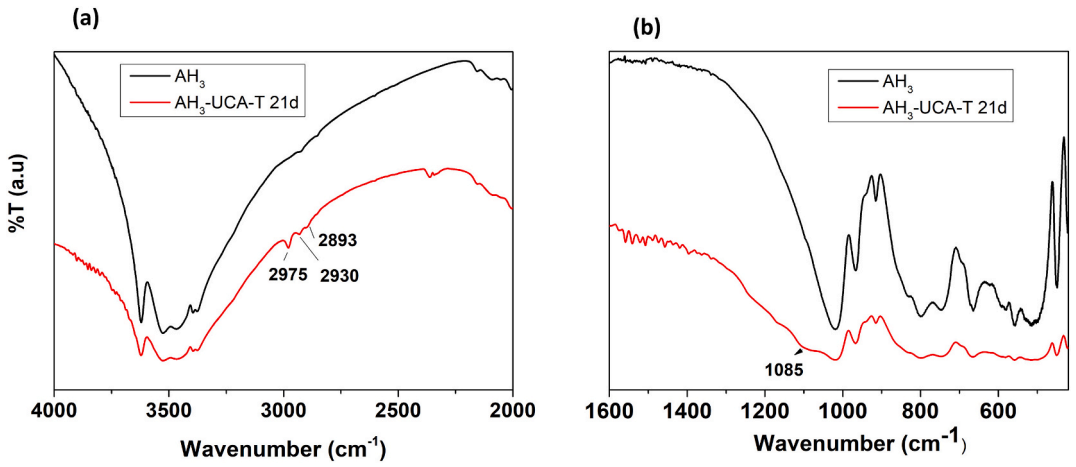

Fig. 23. FTIR spectra for AH_3 and AH_3-UCA-T-21d: (a) 4000 cm^{-1} to 2000 cm^{-1} region; and (b) 1700 cm^{-1} to 450 cm^{-1} region.

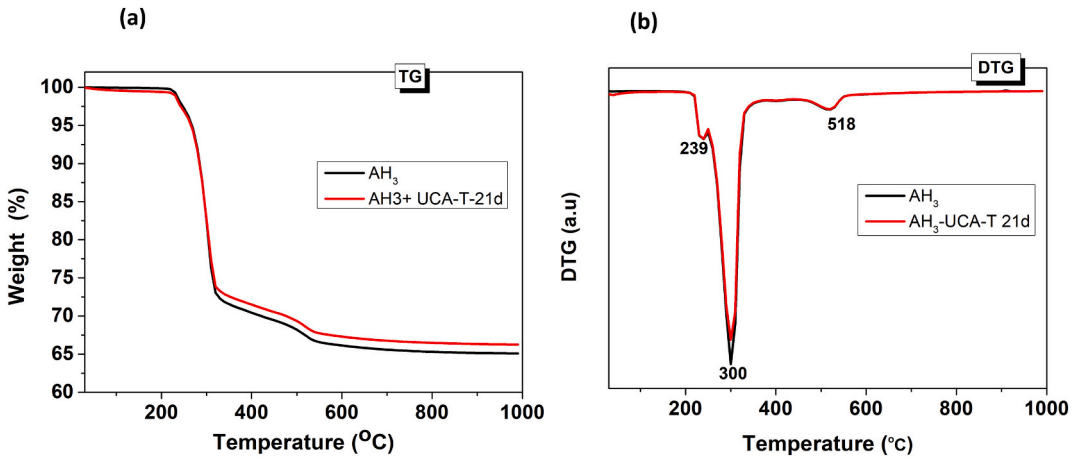

Fig. 24. (a) TG and (b) DTG curves for AH_3 and AH_3-UCA-T-21d.

4. Conclusions

This work studies the interaction of an impregnation product, based on oligomeric alkoxysilanes (UCA-T), with a number of different cementitious phases. These cementitious phases modify the traditional standard hydrolysis-condensation of the UCA-T product, yielding products other than a silica xerogel. More specifically, the conclusions drawn from the study of the interaction between the product and the synthetic phases are as follows.

- All the substrates analysed stimulated alkoxysilane hydrolysis under the test conditions due to their basicity, although AH_3 did so to a lesser extent. The high pH of some phases is able to cleave the Si—O bonds in the oligomeric alkoxysilane units.
- Portlandite reacted chemically with the alkoxysilane, causing cleavage of the Si-O-Si bonds in the oligomeric alkoxysilane units, which in turn interact with the Ca generating C-S-H gels with short Si—O chain length.
- Synthetic C-S-H gel interacted with the hydrolysed silica monomers in the treatment, inducing MLC lengthening, while the remaining oligomers condensed to form three-dimensional silica systems.
- The co-existence of portlandite and C-S-H in the sample (such as in SP-UCA-T-21d) stimulated not only siloxane hydrolysis but also Si-O-Si bond rupture in the oligomers, yielding hydroxylated Si monomers that interacted with the existing C-S-H gel, lowering its mean Ca/Si ratio and increasing the mean chain length.
- Ettringite destabilised in the presence of the product, generating gypsum and AH_3. The silica oligomers in UCA-T interacted with the Al in ettringite, taking it up in tetrahedral positions and generating an aluminosilicate gel with more polymerised structures (Q^3(nAl) or Q^4(nAl) environments).
- In the presence of the UCA-T, calcium monocarboaluminate underwent slight decomposition to amorphous carbonates and an alumina gel.
- Katoite partially decomposed during its interaction with UCA-T, yielding amorphous reaction products that could not be clearly identified.
- Due to the low pH in AH_3 (gibbsite) the hydrolysis of the UCA-T product is less favourable and the substrate remained unaltered.

The present findings show that not only portlandite but all the other cement hydrates except AH_3, interact with alkoxysilanes (one of the most common chemical reagents in commercial products used as concrete surface consolidants), generating a number of stable phases as reaction products. On those grounds, future research might address the compatibility between the aforementioned stable phases and the overall effect of such consolidants on the properties of the surfaces treated.

CRediT authorship contribution statement

MTBV and IGL conceived of the presented idea.
IGL and PCQ carried out the experiments.

IGL wrote the manuscript with support from MTB, RZ and MJM.

All authors discussed the results and contributed to the final manuscript.

Declaration of competing interest

The authors confirm that there are no known conflicts of interest associated with this publication.

Acknowledgements

This research was funded by the European Union's Horizon 2020 - Research and Innovation Framework Programme under grant no. 760858 (Innovaconcrete project), by the Regional Government of Madrid (TopHeritage-CM; S2018/NMT_4372) and by the Spanish Government/FEDER-EU under research project MAT2017-84228-R. Dr. Paula M. Carmona-Quiroga's participation was supported by the Spanish Ministry of Economy and Competitiveness and the European Regional Development Fund under project BIA2015-73237-JIN (MINECO/ERDF; EU). Authors thank the support of the PTI-PAIS platform. Fig. 6

Appendix A. Supplementary data

Supplementary data to this article can be found online at https://doi.org/10.1016/j.cemconres.2020.106351.

References

[1] R. Villegas, R. Baglioni , M. Sameno, Metodología de diagnóstico y evaluación de tratamientos para la conservación de los edificios históricos. Ed. Comares. (2003) Granada (España).
[2] A. Sierra-Fernandez, L.S. Gomez-Villal, M.E. Rabanal, R. Fort, New nanomaterials for applications in conservation and restoration of stony materials: a review, Materiales de Construcción 67 (325) (2017), e107, https://doi.org/10.3989/mc.2017.07616.
[3] F. Casadio, L. Toniolo. Polymer treatments for stone conservation: methods for evaluating penetration depth. Journal of American Institute for Conservation 43 (1):3e (2004) American Institute for Conservation 43(1):3 doi: https://doi.org/10.2307/3179848.
[4] F. Rubio, J. Rubio, J.L Oteo, A FT-IR study of the hydrolysis o tetraethylorthosilicate (TEOS). Spectrosc Lett 31 (1998):199–219. doi:https://doi.org/10.1080/00387019808006772.
[5] G.W. Scherer, G.S. Wheeler, Silicate consolidants for stone, Key Eng. Mater. 391 (2009) 1–25, https://doi.org/10.4028/www.scientific.net/KEM.391.1.
[6] G. Parashar, D. Srivastava, P. Kumar, Ethyl silicate binders for high performance coatings. Progress in Organic Coatings 42 (2001)1–14 doi: https://doi.org/10.1016/S0300-9440(01)00128-X.
[7] G. Wheeler, Alkoxysilanes and the consolidation of stone, in: Research in Conservation, The Getty Conservation Institute, Los Angeles, 2005.
[8] M.J. Mosquera, J. Pozo, L. Esquivias, Stress during drying of two stone consolidants applied in monumental conservation, J. Sol Gel Sci. Technol. 26 (2003) 1227–1231, https://doi.org/10.1023/A:1020776622689.
[9] G.W. Scherer, G.E. Wheeler, in Proc. 4th International Symposium on the Conservation of Monuments in the Mediterranean ,vol. 3, edited by A. Moropoulou, F. Zezza, E. Kollias, and I.Papachristodoulou (1997), Rhodes, 355.
[10] C. Miliani, M.L. Velo-Simpson, G.W. Scherer, Particle-modified consolidants: a study on the effect of particles on sol-gel properties and consolidation effectiveness, J. Cult. Herit. 8 (2007) 1–6, https://doi.org/10.1016/j.culher.2006.10.002.
[11] M.J. Mosquera, M. Bejarano, N. de la Rosa-Fox, L. Esquivias. Producing crack-free colloid-polymer hybrid gels by tailoring porosity. Langmuir 19 [3](2003) 951–957 doi: https://doi.org/10.1021/la0265981.
[12] M. J. Mosquera, D. M. de los Santos, L. Valdez-Castro, L. Esquivias. New route for producing crack-free xerogels: obtaining uniform pore size. Journal of Non-Crystalline Solids 354 (2008) 645–650 doi:https://doi.org/10.1016/j.jnoncrysol.2007.07.095.
[13] M.J. Mosquera, A. Montes, D.M. de los Santos, Method of Strengthening Stone and Other Constructions Materials, 2008. US2008/0209847A1.
[14] D.S. Facio, M. Luna, M.J. Mosquera, Facile preparation of mesoporous silica monoliths by an inverse micelle mechanism, Microporous and Mesoporous Materials 247 (2017) 166–176, https://doi.org/10.1016/j.micromeso.2017.03.041.
[15] F. Elhaddad, L.A.M. Carrascosa, M.J. Mosquera, Long-term effectiveness, under a mountain environment, of a novel conservation nanomaterial applied on limestone from a Roman archaeological site, Materials (Basel) 11, 2018, https://doi.org/10.3390/ma11050694.
[16] A.M. Barberena-Fernández, P.M. Carmona-Quiroga, M.T. Blanco-Varela, Interaction of TEOS with cementitious materials: chemical and physical effects, Cem. Concr. Compos. 55 (2015) 145–152, https://doi.org/10.1016/j.cemconcomp.2014.09.010.
[17] B. Pigino, A. Leemann, E. Franzoni, P. Lura, Ethyl silicate for surface treatment of concrete – part II: characteristics and performance, Cem. Concr. Compos. 34 (2012) 313–332, https://doi.org/10.1016/j.cemconcomp.2011.11.021.
[18] A. Moropoulou, A. Cakmak, K.C Labropoulos, R. Van Grieken,K. Torfs , Accelerated microstructural evolution of a calcium–silicate–hydrate (C–S–H) phase in pozzolanic pastes using fine siliceous sources: comparison with historic pozzolanic mortars. Cement and Concrete Research 34 (2004)1–6 doi:https://doi.org/10.1016/S0008-8846(03)00187-X.
[19] F. Sandrolini, E. Franzoni , B. Pigino Ethyl silicate for surface treatment of concrete. Part I: pozzolanic effect of ethyl silicate. Cement and Concrete Composites 34 (2012) 306–312 doi:https://doi.org/10.1016/j.cemconcomp.2011.12.003.
[20] R. Zarzuela, M. Luna, L.M. Carrascosa, M. P. Yeste, I. Garcia-Lodeiro, M. T Blanco-Varela, M. A. Cauquic, J. M. Rodríguez-Izquierdo, M. J. Mosquera. Producing C-S-H gel by reaction between silica oligomers and portlandite: a promising approach to repair cementitious materials. Cement and Concrete Research. 130 (2020) 106008. doi:https://doi.org/10.1016/j.cemconres.2020.106008.
[21] I.F Sáez del Bosque, M. Martín-Pastor M, S. Martínez Ramírez, M.T Blanco-Varela Effect of temperature on C_3S and C_3S + nanosilica hydration and C-S-H gel structure J. American Ceramic Society J. Am. Ceram. Soc. 96 [3] (2013) 957–965 doi: https://doi.org/10.1111/jace.12093.
[22] C. Kapridaki, P. Maravelaki-Kalai, TiO_2–SiO_2–PDMS nano-composite hydrophobic coating with self-cleaning properties for marble protection, Prog. Org. Coat. 76 (2013) 400–410, https://doi.org/10.1016/J.PORGCOAT.2012.10.006.
[23] M. Montes, E. Pato, P.M. Carmona-Quiroga, M.T. Blanco-Varela, Can calcium aluminates activate ternesite hydration? Cem. Concr. Res. 103 (2018) 204–215, https://doi.org/10.1016/j.cemconres.2017.10.017.
[24] I.F. Sáez del Bosque, S. Martínez-Ramírez, M.T. Blanco-Varela, FTIR study of the effect of temperature and nanosilica on the nanostructure of C-S-H gel formed by tricalcium silicate hydration, Constr. Build. Mater. 52 (2014) 314–323, https://doi.org/10.1016/j.conbuildmat.2013.10.056.
[25] L.J. Struble, Synthesis and characterization of ettringite and related phases, Proc. 8th Int. Cong. Chem. Cem., Rio de Janeiro 6 (1986) 582–588.
[26] P.M. Carmona-Quiroga, M.T. Blanco-Varela, Ettringite decomposition in the presence of barium carbonate, Cem. Concr. Res. 52 (2013) 140–148, https://doi.org/10.1016/j.cemconres.2013.05.021.
[27] E. Franzoni, G. Graziani, E. Sassoni, TEOS-based treatments for stone consolidation: acceleration of hydrolysis–condensation reactions by poulticing Journal of sol-gel science and technology 74 [2] (2015)398-405doi: https://doi.org/10.1007/s10971-014-3610-3.
[28] F. Xu W. Zeng, D. Li, Recent advance in alkoxysilane-based consolidants for stone. Progress in organic coatings, 127 (2019) 45–54 doi : https://doi.org/10.1016/j.porgcoat.2018.11.003.
[29] A.M. Barberena-Fernández, Conservación de esculturas de hormigón. Efecto de consolidantes en pastas y morteros de cemento, Universidad Complutense de Madrid, (2016) Spain.
[30] M. P Besland. Synthèse et caractérisation de composés hétéropolisiloxanes. Application aux membranes d'hiperfiltration, Doctoral Thesis, University of Montpellier. (1989) France.
[31] L. Desgranges, D. Grebille, G. Calvarin, G. Chevrier, N. Floquet, J.-C. Niepce, Hydrogen thermal motion in calcium hydroxide: $Ca(OH)_2$, Acta Crystallogr. Sect. B (1993) 812–817, https://doi.org/10.1107/S0108768193003556.
[32] S. Martínez-Ramírez, M.T. Blanco-Varela, Thermodinamically stable phases in the CaO-SiO_2-Al_2O_3-$CaSO_4$-H_2O closed system at 25 °C. Application to cementitious systems, Materiales de construcción 59 (2009) 31–33, https://doi.org/10.3989/mc.2009.45407.
[33] J. A. Gadsden. The Infrared Spectra of Minerals and Related Inorganic Compounds. London (Butterworths) (1975) United Kingdom.
[34] P. Yu, R. J. Kirkpatrick, B. Poe, P. F. McMillan , X. Cong , Structure of calcium silicate hydrate (C-S-H): near-, mid-, and far-infrared spectroscopy, J. Am. Ceram. Soc., 82 [3] (1999)742–48 doi:https://doi.org/10.1111/j.1151-2916.1999.tb01826.x.
[35] V. C Farmer, The Infrared Spectra of Minerals, Mineralogical Society, V4, (1974) Aberdeen United Kingdom.
[36] B. Lothenbach. P. Durdziński and K. De Weerdt, Thermogravimetric analysis, in A Practical Guide to Microstructural Analysis of Cementitious Materials, Ed. By Karen Scrivener, Ruben Snellings and Barbara Lothenbach, CRC Press, Taylor & Francis Group, (2016) United Kingdom.
[37] G. Villain, M. Thiery, G. Platret, Measurement methods of carbonation profiles in concrete: thermogravimetry, chemical analysis and gammadensimetry, Cem. Concr. Res. 37 (2007) 1182–1192, https://doi.org/10.1016/j.cemconres.2007.04.015.
[38] I.G. Richardson, G.W. Groves, Models for the composition and structure of calcium silicate hydrate (C-S-H) gel in hardened tricalcium silicate pastes, Cem. Concr. Res. 22 (1992) 1001–1010, https://doi.org/10.1016/0008-8846(92)90030-Y.
[39] C. Roosz, P. Vieillard, P. Blanc, S. Gaboreau, H. Gailhanou, D. Braithwaite, V. Montouillout, R. Denoyel, P. Henocq, B. Madé, Thermodynamic properties of C-S-H, C-A-S-H and M-S-H phases: results from direct measurements and predictive modelling, Appl. Geochem. 92 (2018) 140–156, https://doi.org/10.1016/j.apgeochem.2018.03.004.

[40] S. Stronach, N.L Walker, D.E Macphee, F.P Glasser, Reactions between cement and As (III) oxide: the system CaO-SiO_2-As_2O_3-H_2O at 25 °C. Waste management 17 (1997) 9–13 doi:https://doi.org/10.1016/S0956-053X(97)00029-9.
[41] H. F. W Taylor, Chemistry of Cement, Ed. Thomas Telford Publishing, Aberdeen (2004) United Kingdom.
[42] I. Garcia-Lodeiro, A. Fernandez-Jimenez, I. Sobrados, J. Sanz, A. Palomo, C–S–H gels: interpretation of ^{29}Si MAS-NMR spectra, J. Am. Ceram. Soc. 95 (2012) 1440–1446, https://doi.org/10.1111/j.1551-2916.2012.05091.x.
[43] G. Engelhardt, D. Michel, High Resolution Solid State NMR of Silicates and Zeolites, Wiley and Sons, New Delhi, India, 1987.
[44] I.G. Richardson, The nature of C-S-H in hardened cements, Cem. Concr. Res. 29 (1999) 1131–1147, https://doi.org/10.1016/S0008-8846(99)00168-4.
[45] T.F. Sevelsted, J. Skibstes, Carbonation of C–S–H and C–A–S–H samples studied by ^{13}C, ^{27}Al and ^{29}Si MAS NMR spectroscopy, Cem. Concr. Res. 71 (2015) 56–65, https://doi.org/10.1016/j.cemconres.2015.01.019.
[46] A. Ayuela, J J. S. Dolado, I. Campillo, Y. R. de Miguel, E. Erkizia, D. Sánchez-Portal and A. Rubio A. Porro, P. M. Echenique, Silicate chain formation in the nanostructure of cement-based materials, J. Chem. Phys. 127 (2007) 164710 doi: https://doi.org/10.1063/1.2796171.
[47] T. Vazquez Moreno, Contribucion al estudio de las reacciones de hidratación del cemento portland por espectroscopia infraroja, Doctoral Thesis, Universidad Complutense de Madrid, (1975) Spain.
[48] A.E. Moore, H.F.W. Taylor, Crystal structure of ettringite, Nature 218 (1968) 1048–1049, https://doi.org/10.1038/2181048a0.
[49] R.B. Perkins. The Solubility and Thermodynamic Properties of Ettringite, Its Chromium Analogs ABD Calcium Aluminum Monochromate ($3CaO{\cdot}Al_2O_3{\cdot}CaCrO4\ nH_2O$). Doctoral Thesis. (2000) Portland State University.
[50] C.J. Warren, E.J. Reardon, The solubility of ettringite at 25°C, Cem. Concr. Res. 24 (1994) 1515–1524, https://doi.org/10.1016/0008-8846(94)90166-X.
[51] T. Vázquez Moreno, Aplicaciones prácticas de la espectroscopia de absorción infrarroja en el estudio de los crudos, del clinker y del cemento portland anhidro, Mater. Constr. 175 (1980) 45–58, https://doi.org/10.3989/mc.1980.v30.i179.1052.
[52] V.S. Ramachandran, R.M. Paroli, J.J. Beaudoin, A.H. Delgado, Handbook of Thermal Analysis of Construction Materials, Noyes Publications/William Andrew Publishing, United States of America, 2002.
[53] T. Grounds, H.G. Midgley, D.V. Nowell, The use of thermal methods to estimate the state of hydration of calcium trisulphoaluminate hydrate $3CaO{\cdot}Al_2O_3{\cdot}3SO_4{\cdot}nH_2O$, Thermochim. Acta 85 (1985) 215–218, https://doi.org/10.1016/0040-6031(85)85567-2.
[54] T. Grounds, G. Midglbya, V. Novell, Carbonation of ettringite by atmospheric carbon dioxide, Thermochim. Acta 135 (1988) 347–352, https://doi.org/10.1016/0040-6031(88)87407-0.
[55] S. Steiner, B. Lothenbach, A. Borgschulte, T. Proske, F. Winnefeld, Effect of relative humidity on the carbonation rate of portlandite, calcium silicate hydrates and ettringite, in: Ibausil 2018, At Weimar, 2018.
[56] J. Skibsted, High resolution solid-state nuclear magnetic resonance spectroscopy of Portland-based systems; in A Practical Guide to Microstructural Analysis of Cementitious Materials, Ed. K. Scrivener, R. Snellings, B. Lothenbach, CRC Press (2016).
[57] H.J. Andersen, J. Jakobsen, J. Skibsted, Characterization of white portland cement hydration and the C-S-H structure in the presence of sodium aluminate by ^{27}Al and ^{29}Si MAS NMR spectroscopy, Cem. Concr. Res. 34 (2004) 857–868, https://doi.org/10.1016/j.cemconres.2003.10.009.
[58] M. François, G. Renaudin, O. Evrard. A cementitious compound with composition $3CaO{\cdot}Al_2O_3{\cdot}CaCO_3{\cdot}11H_2O$. Acta Crystallographica Section C (1998) 1214–1217. doi:https://doi.org/10.1107/S0108270198004223.
[59] T. Matschei, B. Lothenbach, F.P. Glasser. Thermodynamic properties of Portland cement hydrates in the system $CaO–Al_2O_3–SiO_2–CaSO_4–CaCO_3–H_2O$. Cement and Concrete Research 37 (2007) 1379–1410doi:https://doi.org/10.1016/j.cemconres.2007.06.002.
[60] M. Horgnies, J. J. Chen , C. Bouillon, Overview about the use of Fourier Transform Infrared spectroscopy to study cementitious materials, 252 Materials Characterisation VI, WIT Transactions on Engineering Sciences, 77, (2013) WIT Press.
[61] R. Gabrovšek, T. Vuk, V. Kaučič, The preparation and thermal behavior of calcium monocarboaluminate, Acta Chim. Slov. 55 (2008) 942–950. http://www.dlib.si/?URN=URN:NBN:SI:DOC-FZGEQDC.
[62] B.A Kolesov, C.A Geiger, The vibrational spectrum of synthetic hydrogrossular (katoite) $Ca_3Al_2(O_4H_4)_3$: a low-temperature IR and Raman spectroscopic study, American Mineralogist, 90 (2005) 1335–1341 doi: https://doi.org/10.2138/am.2005.1622.
[63] M. Földvári, Handbook of Thermogravimetric System of Minerals and Its Use in Geological Practice, Geological Institute of Hungary — Kiadja a Magyar Állami Földtani Intézet, Budapest, Hungary, 2011.
[64] J.M. Rivas Mercury, P. Pena, A.H. De Aza, X. Turrillas, I. Sobrados, J. Sanz, Solid-state ^{27}Al and ^{29}Si NMR investigations on Si-substituted hydrogarnets, Acta Mater. 55 (2007) 1183–1191, https://doi.org/10.1016/j.actamat.2006.09.032.
[65] W. A. Deer, R. A. Howie, J. Zussman. An introduction to the rock-forming minerals. Mineralogical Society of Great Britain and Ireland, 3rd edition, (2013). https://pubs.geoscienceworld.org/books/book/952/chapter/106865161/Gibbsite-Al-OH-3.
[66] N.V. Chukanov, Infrared Spectra of Mineral Species, Vol 1, Springer, United States, New York, 2014.